HOKKAIDO UNIVERSITY

Title	Quartz fabrics in Alteration Zones Surrounding the Hitachi Copper Deposits, Abukuma Plateau, Japan
Author(s)	Watanabe, Jun
Citation	Journal of the Faculty of Science, Hokkaido University. Series 4, Geology and mineralogy, 16(2-3), 145-192
Issue Date	1974-11
Doc URL	http://hdl.handle.net/2115/36032
Type	bulletin (article)
File Information	16(2-3)_145-192.pdf

Instructions for use

Hokkaido University Collection of Scholarly and Academic Papers : HUSCAP

QUARTZ FABRICS IN ALTERATION ZONES SURROUNDING THE HITACHI COPPER DEPOSITS, ABUKUMA PLATEAU, JAPAN

by

Jun WATANABE

(With 38 Text-figures and 1 folded map)

(Contribution from the Department of Geology and Mineralogy,
Faculty of Science, Hokkaido University, No. 1375)

CONTENTS

Abstract

As the result of tectonic and metasomatic effects, the alteration zones around the Hitachi copper deposits, one of the largest cupriferous iron sulphide ore deposits in Japan, are remarkably well-developed.

In order to study the circumstances of alteration in detail, the writer has employed the techniques of petrofabric analyses.

The petrofabric patterns obtained are characterized by duplicate spheroidal symmetry (according to the definition by FAIRBAIRN, 1949) around an axis which coincides with the plunge of the shoot of the ore bodies.

In the zone of alteration, which is very quartz rich, many quartz grains are oriented in a "Japanese twin relation" with neighbouring grains, as was previously shown in the Nishidohira gneiss fabrics (WATANABE, 1971).

Furthermore, an intimate coordination relationship exists not only between quartz grains, but also between quartz and pyrite, and pyrite aggregates.

Introduction

The Abukuma Plateau lying on the outer margin (Pacific side) of northeast Honshu extends about 300 km from north to south and is 70 km wide. It is one of the major tectonic units of the Japanese Islands. The plateau includes some fascinating geological problems as for example those concerning the orogenic and metamorphic history of the area, the age of the various units, and the nature of the associated ore deposits.

In the earliest studies, all the metamorphism were assumed to be of Precambrian age (KOTO, 1892). However, certain polymetamorphic features were noticed later by WATANABE (1920, 1921). A group of high grade metamorphics, probably of Precambrian age, was distinguished from a group of low grade metamorphics by SUGI (1935). The latter may have been derived from Palaeozoic rocks and/or from pre-existing gneisses and amphibolites as a result of diaphtoritic processes.

The writer's own studies have revealed a complex metamorphic history for the region of the Hitachi mine, located at the southern end of the Abukuma Plateau (WATANABE, 1971; WATANABE and BIKERMAN, 1971). It seems probable that the Hitachi copper deposits are a product of rejuvenation of the basement complex of the area brought about by tectonic movements during the Abean (≒Variscan) and Indosinian orogeneses.

The present study is connected with the quartz fabrics of rocks in the alteration zones which are associated with the copper mineralization.

Geological setting of the mineralization

Along the western margin of the Abukuma Plateau, a broad zone of major structural distrubance, called the Tanakura structural belt, follows a NNW-SSE trend and is 3–4 km in width. A basement complex, of probable Precambrian age, consisting of the Nishidohira and the Tamadare formations is intermittently exposed as blocks in and around this structural belt. Details concerning the metamorphic history of these formations have been given previously (WATANABE, 1971). Some amphibolitic masses similar to those of the Tamadare formation are also seen in the eastern part of the area, where the weakly metamorphosed Palaeozoic rocks are well developed. In this case the wedge-shaped sheared blocks of the Tamadare formation are within the zones of faulting or shearing.

Stratigraphically, the Palaeozoic formation of the region seems to represent a time interval extending from Devonian to Upper Permian. The lowermost Palaeozoic unit is the Kamine formation. This sequence is composed of acidic pyroclastics such as leptite and hälleflinta, accompanied by a few thin intercalating diabasic tuff seams. The Kamine is developed extensively in the northwestern part of the district. In general, it shows a NE strike and nearly vertical dip. Although the writer has not completed the geological map and defined the stratigraphical succession in detail, it seems clear that the hälleflinta member overlies the leptite member in the succession. Overlying both is the Okadoya formation. This unit is chiefly composed of diabasic pyroclastics with intercalating pillow lava, slate, sandstone, and thin layers of limestone, conglomerate and acidic tuff. It shows tectonic features similar to those seen in the Kamine formation. Strongly sheared or mylonitized zone follows a NE-SW trend along the boundary between the Kamine and the Okadoya formations (see, Fig. 39 Alteration Map). In the eastern part of this district, outside the area covered by the map, the Okadoya formation is overlain unconformably by a fossiliferous limestone sequence of Upper Viséan age, called the Sugimoto formation. This formation is correlated with the Onimaru series of the Kitakami mountains. Although both of the older formations are partially metamorphosed, at most to green schist facies, the Sugimoto formation shows no sign of regional metamorphism. Accordingly, the metamorphism may be correlated to the Shizu phase of the Abean Orogenic Movement in Japan established by MINATO (1968). This event, in turn has been correlated with Pre-Chesterian or Pre-Upper Viséan time. The Upper Permian formation intercalating the Usuginu conglomerate, redefined by the writer as the Ayukawa formation, is widely developed still further east. Lower and Middle Permian units are apparently absent.

A huge intrusion, which is comparable both lithologically and in mode of intrusion, to the Triassic granodiorite masses occuring in Northeastern Japan, intrudes all of the above-mentioned formations of this area. This mass, named the Daioh-in sheared granodiorite, is strongly sheared and altered. The Indosinian Orogenic Movement which accompanied this intrusion imprinted an extremely complicated structural and metamorphic pattern on this district which is as yet only very imperfectly understood. There was not only severe tectonic disturbance such as folding, faulting and shearing, but also thermal metamorphism and mineralization which affected all of the above-mentioned formations. Small masses of trondhjemite, granophyre, microdiorite and metasomatic gabbro were intruded as the forerunners of this intrusion. A large volume of Neocomian granodiorite intruded in the northwest part of this district, also inflicted thermal and tectonic effects upon the surroundings. Serpentinites masses were intruded, as the forerunners of this intrusion, along sheared zones as a general NE–SW trend.

Zone of alteration

The zone of alteration which is associated with the ore deposits is well-developed and has well defined boundaries. It is over 8 km long and extends southwestwards byond the quadrangle of the Alteration Map. In the northeast it disappears abruptly immediately north of the mine, owing to an intrusion of Neocomian granodiorite. Noteworthy ore bodies such as Irishiken, Fujimi, Kamine, Chusei, Honkoh, Akazawa and Takasuzu are all lying in a mineralized zone, 4 km long and 1.5 km in width, which represents the most strongly altered part amidst the alteration zone.

This zone is composed of a great number of units of smaller dimensions arranged en echélon each having a span of several hundred metres. Each unit is commonly composed of more than one alteration facies. The following facies are found: (1) chlorite-sericite-quartz, (2) sericite-quartz-pyrite, (3) sericite-quartz-andalusite-pyrite, (4) cordierite-quartz-pyrite, (5) anthophyllite-quartz-pyrite, (6) anthophyllite-cordierite-quartz-pyrite, and (7) anthophyllite-cordierite rock facies with skarn assemblages. There are some places where all the facies are closely associated and appear to have formed simultaneously, but in general two trends can be identified in these units, both are metasomatic. In the first facies (1) is replaced by (2) and further facies (3), and in the second facies (4) is replaced by (5) and (6) followed by facies (7). The two trends are distinctly different in spatial disposition. According to a geological profile based on underground maps, the former (first, second and third facies) is at a higher level than the latter. This suggests that the former is, in general, a shallower facies than the latter.

The alteration which took place in or around sheared zones with a NE–SW trend, where the fissility and the lineation are very well-developed, is easily distinguished from unaltered country rocks on the basis of tectonic appearance. The wall rocks are nearly massive or very weakly schistose, what little fissility and lineation they show is of a different tectonic style. On the whole, it may be concluded that the tectonic force operating along the sheared zones through the whole alteration period resulted in lateral movement in a NE–SW direction.

As alteration processes advanced, the rocks became strongly metasomatized as, for example facies (3) rocks which are full of porphyroblastic andalusite spots or facies (6) and (7) which contain large amounts of porphyroblastic anthophyllite and cordierite, with small amounts of sillimanite, corundum, anti-perthitic feldspar and locally lime-silicate minerals such as garnet, diopside and hedenburgite. Generally speaking, from chemical considerations alone, it is reasonable to assume magnesium metasomatism to have taken place towards the end of the period of alteration.

Results of quartz fabric analyses

Microscopic fabric analyses on the preferred orientation of quartz were carried out for each facies. The analyses were made by measuring the orientation of 3,000–4,000 individual quartz grains in each section. Micro-

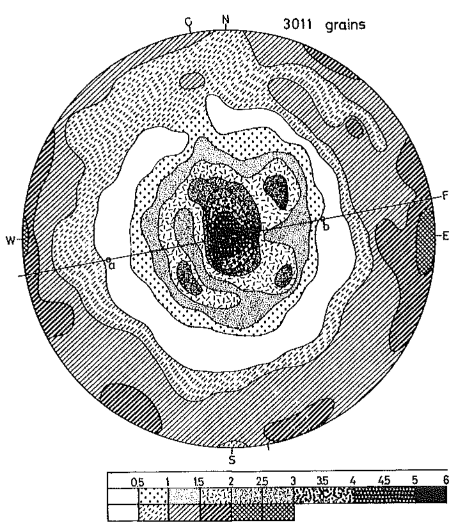

Fig. 1 A representative quartz fabric pattern of sericite-quartz-andalusite-pyrite rock facies. F is the foliation plane. a, b and c are of fabric axis. The upper column is the concentration degree of the inner circle, the lower is one of the outer circle.

photographs were taken of each section, and all the quartz grains were numbered consecutively and then measured to avoid any omissions.

(1) *sericite-quartz-andalusite-pyrite rock facies:*

Fig. 1 shows a representative pattern of the sericite-quartz-andalusite-pyrite facies. Chlorite-sericite-quartz and sericite-quartz-pyrite facies gave similar patterns.

This pattern is characterized by a duplicate spheroidal symmetry (as defined by FAIRBAIRN, 1949). The maximum coincides with the axis of the shoot of the ore bodies, as shown in Fig. 1. There are in addition a few sub-maxima separated by angles of 25° to 26° from the maximum. Macrotectonic axes a and b, projected on the pattern, are not necessarily in accordance with the symmetry of the pattern.

The relationship between orientation of the individual grains and position in the thin section has also been studied.

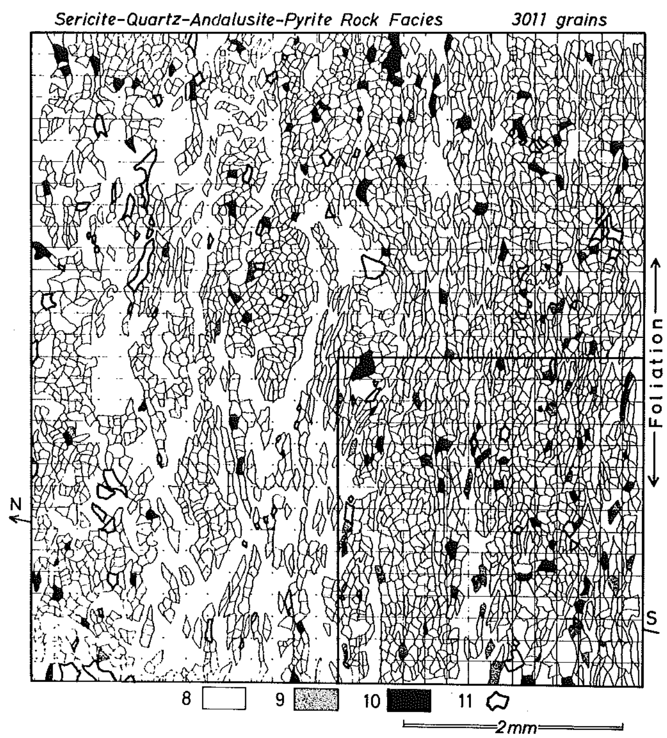

Fig. 2 A measured area in a thin section of sericite-quartz-andalusite-pyrite rock facies for quartz fabric analysis. Furthermore, within a small squared area the more detailed analyses as shown in Fig. 3 and Fig. 22 are carried out. The vacant matrix consists of sericite, plagioclase, and andalusite. 8: measured quartz grains with the definite coordination relation. 9: measured quartz grains without the definite coordination relation. 10: particularly, measured quartz grains plotted to the most concentrated central point of Fig. 1. 11: pyrite grains.

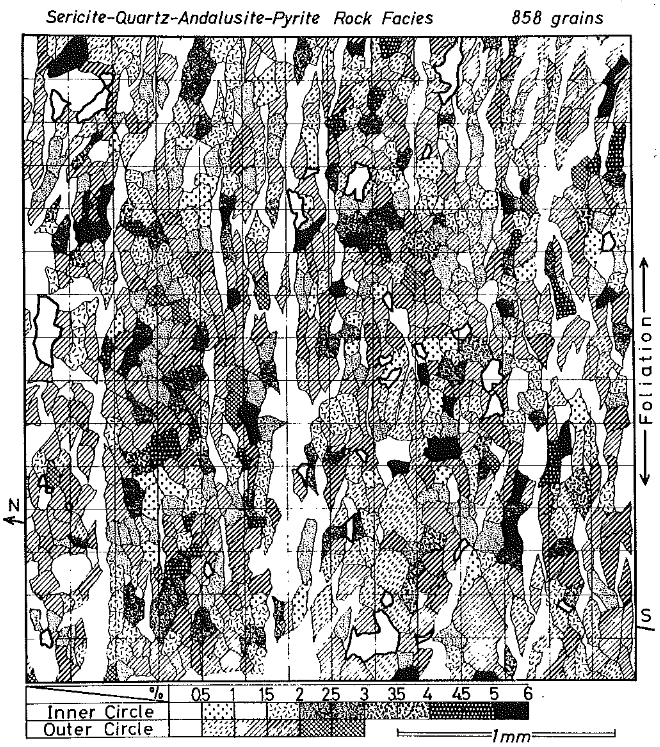

Fig. 3 A.V.A. detailed map of the squared area in Fig. 2.

All quartz grains were classified into one of eleven possible groups according to whether they were plotted in the 1, 1.5, 2, 3, 4, 5 or 6% concentration areas of the inner circle, or the 1, 1.5, 2 or 3% areas of the outer circle (Fig. 1). The distribution of each group in one thin section is shown by differential colouring on microphotographs (Fig. 3). A.V.A. Contour Maps (A plotting method first used in a previous paper, WATANABE, 1971), are made by drawing the statistical contour lines for concentration grade in the respective groups. Plots of this type for both inner and outer circles are shown in Figs. 4a and 4b. The distribution is not uniform throughout the thin section, local concentrations of the respective groups are vividly revealed. There are many small domains formed by aggregation of a few to some tens of grains having similar preferred orientation. The domains have somewhat elongated form and are arranged roughly parallel to the foliation plane. When Figs. 4a and 4b are compared it is seen that they are complementary but have a fringing relation, viz. those grains belonging to the outer circle are exclusively plotted to the areas closely fringed to those of maxima of the inner circle.

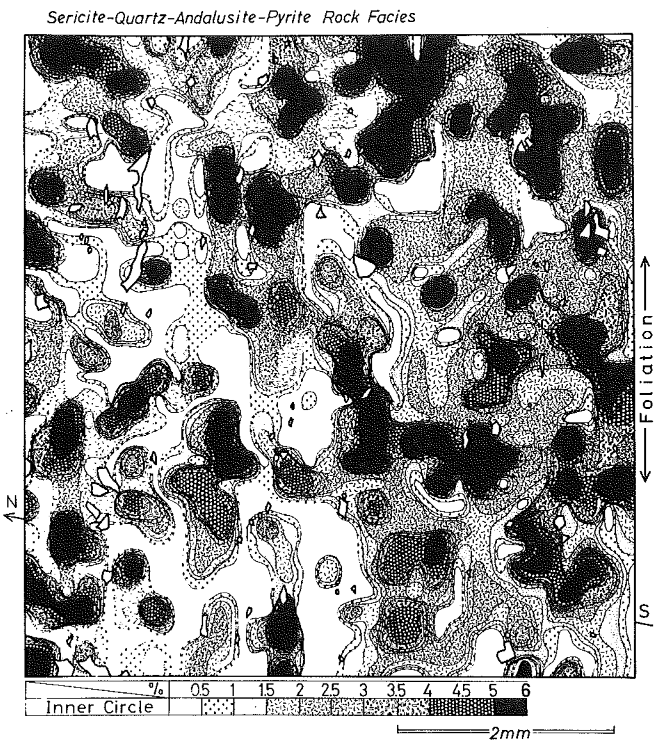

Fig. 4a A.V.A. Contour Map belonging to inner circle of Fig. 1, which is maintained by making the statistical contour lines of concentration grade in respective group.

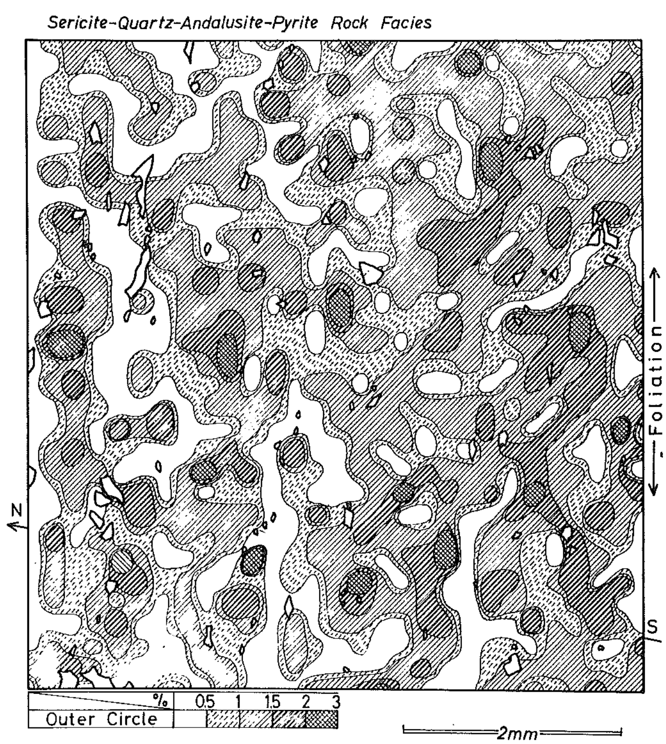

Fig. 4b A.V.A. Contour Map belonging to outer circle of Fig. 1, which is maintained by making the statistical contour lines of concentration grade in respective group.

(2) *cordierite-quartz-pyrite rock facies:*

A representative pattern from this rock facies is given in Fig. 5. The characteristic features of duplicate spheroidal symmetry are again present. An analysis of fabric diagram has also been carried out on this rock facies. A.V.A.

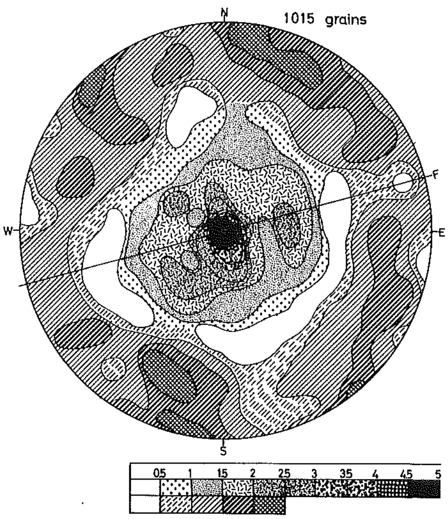

Fig. 5 A representative quartz fabric pattern of cordierite-quartz-pyrite rock facies. The upper column is the concentration degree of the inner circle, the lower is one of the outer circle.

Contour Maps of the inner and outer circles respectively are shown in Figs. 8a and 8b. As before, there are many small domains in these maps formed by aggregation of a few to some tens of quartz grains of similar orientation and again the domains have a somewhat elongated form and are arranged roughly parallel to the foliation plane. When the maximum of Figs. 8a and 8b are compared, they are seen to occupy the different positions just as they did in the first facies.

(3) *anthophyllite-quartz-pyrite rock facies:*

A representative pattern from this rock facies is shown in Fig. 9. Although the duplicate spheroidal symmetry is also evident in this diagram, the concentrations are less well marked.

A.V.A. Countour Maps of the inner and outer circles respectively are shown in Figs. 12a and 12b. There are again many domains formed by aggregation of a few to some tens of quartz grains of similar orientation, and again the domains have somewhat elongated form and arranged roughly parallel to the foliation plane.

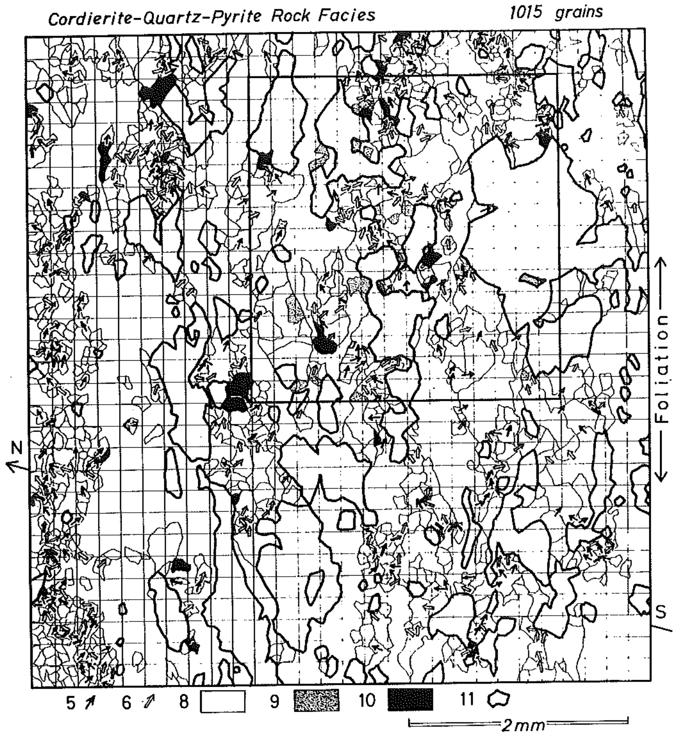

Fig. 6 A measured area in a thin section of cordierite-quartz-pyrite rock facies for quartz fabric analysis. Furthermore, within a small squared area, the more detailed analyses as shown in Fig. 7 and Fig. 24 are carried out. The vacant matrix consists of plagioclase, chlorite and a small amount of anthophyllite. 5: coordination relation at 77°. 6: coordination relation at 84°. 8: measured quartz grains with the definite coordination relation. 9: measured quartz grains without the definite coordination relation. 10: measured quartz grains disposed at the most concentrated central point in Fig. 5. 11: pyrite grains.

(4) *anthophyllite-cordierite-quartz-pyrite rock facies:*

A representative pattern from this rock facies is shown in Fig. 13. The anthophyllite-cordierite rock facies with skarn assemblages gives virtually the same pattern. A.V.A. Contour Maps have again been constructed. The results are presented in Figs. 16a and 16b. Again, there are many elongated domains formed by aggregation of grains with similar orientation but in this case their arrangement is somewhat oblique to the foliation plane. As in previous cases, the domains of high concentration in the two figures are complement each other. It is also noteworthy that most of the domains of high concentration are also located in the immediate neighbourhood of pyrite grains.

Another feature of this facies is grain size variation as shown for example in Fig. 14. In certain areas the aggregates of fine quartz and pyrite have been replaced by coarse grains to give a kind of porphyroblastic texture. The data of Fig. 13 has therefore been replotted 1) in terms of proximity to pyrite and 2) in terms of grain size to give four new diagrams (Figs. 17a, 17b, 17c and 17d). As a result, the following conclusions can be drawn. a) Although the highest concentration on the original diagram is a maximum corresponding to the direction of inclination of the shoot of the ore bodies, there are in addition a few extra maxima superimposed on the rough spheroidal symmetry. b) A comparison of the patterns for the fine and coarse facies shows that the latter is the most strongly oriented attaining 9% and higher in the central area. It must be concluded that quartz grains of the coarse facies which may have grown porphyroblastically at a slightly later stage than those of the fine facies were strongly oriented with the regard to the direction of inclination of the shoot of the ore bodies. The outer circle of the quartz fabric pattern of the coarse facies is not well-developed and be regarded as a remnant structure of the fine facies. c) Judging from the patterns, there is no significant variation in the patterns according to proximity to sulphide minerals.

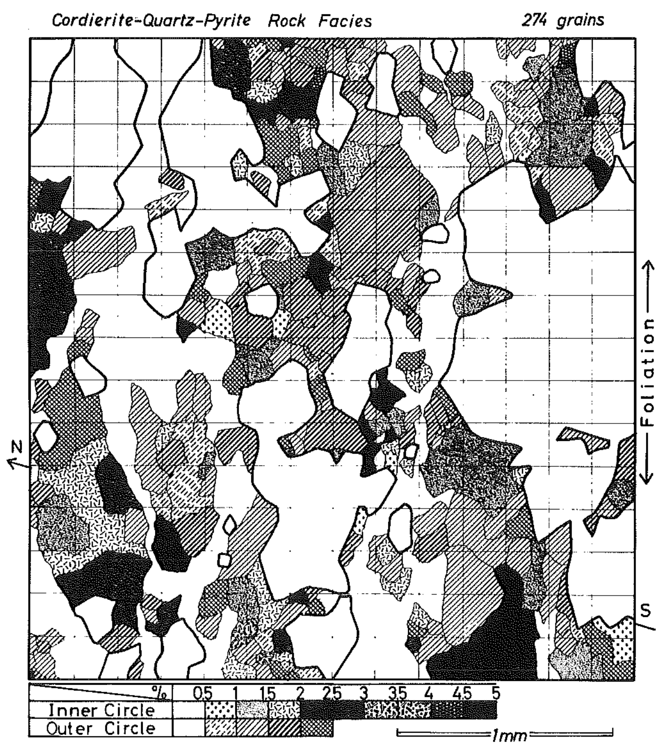

Fig. 7 A.V.A. detailed map of the squared area in Fig. 6.

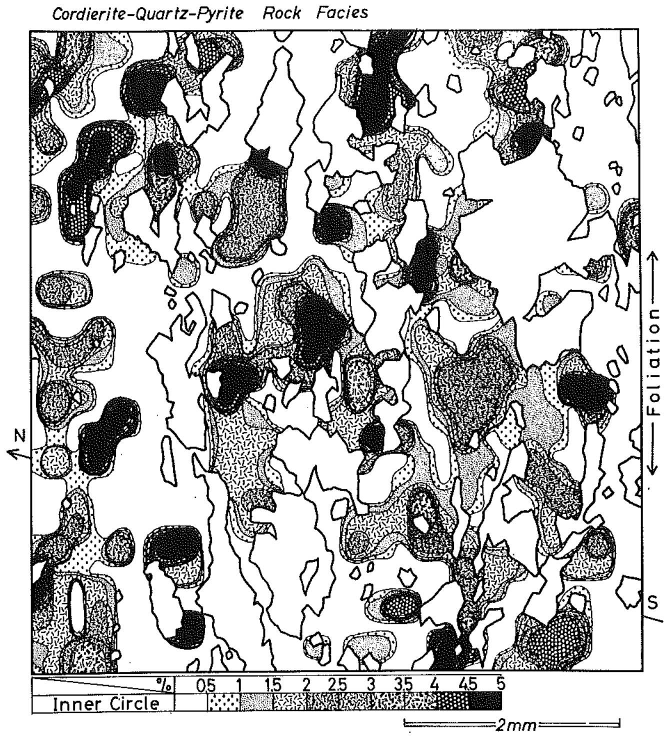

Fig. 8a A.V.A. Contour Map belonging to inner circle of Fig. 5, which is maintained by making the statistical contour lines of concentration grade in respective group.

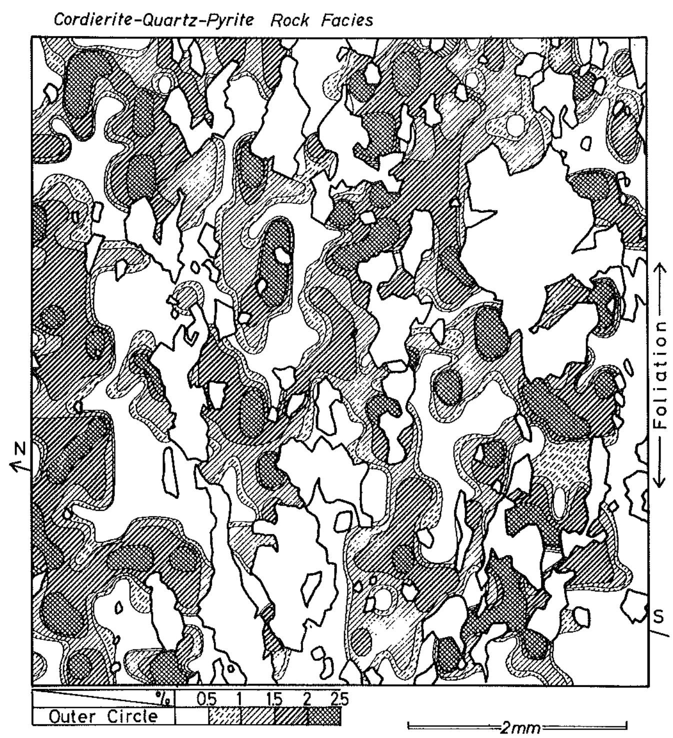

Fig. 8b A.V.A. Contour Map belonging to outer circle of Fig. 5, which is maintained by making the statistical contour lines of concentration grade in respective group.

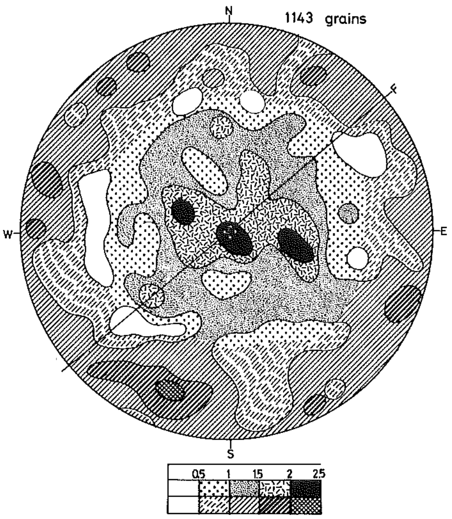

Fig. 9 A representative quartz fabric pattern of anthophyllite-quartz-pyrite rock facies. The upper column is the concentration degree of the inner circle, the lower is one of the outer circle.

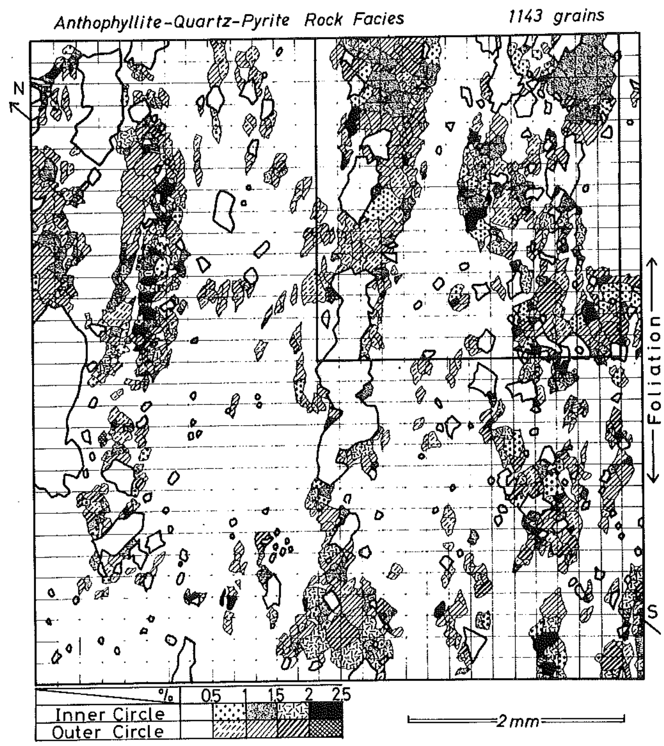

Fig. 10 A measured area in a thin section of anthophyllite-quartz-pyrite rock facies for quartz fabric anslysis and A.V.A. detailed map. Furthermore, within a small squared area, the more detailed analyses as shown in Fig. 11 and Fig. 25 are carried out. The vacant matrix consists of anthophyllite, plagioclase, biotite, chlorite, a small amount of cordierite and sillimanite.

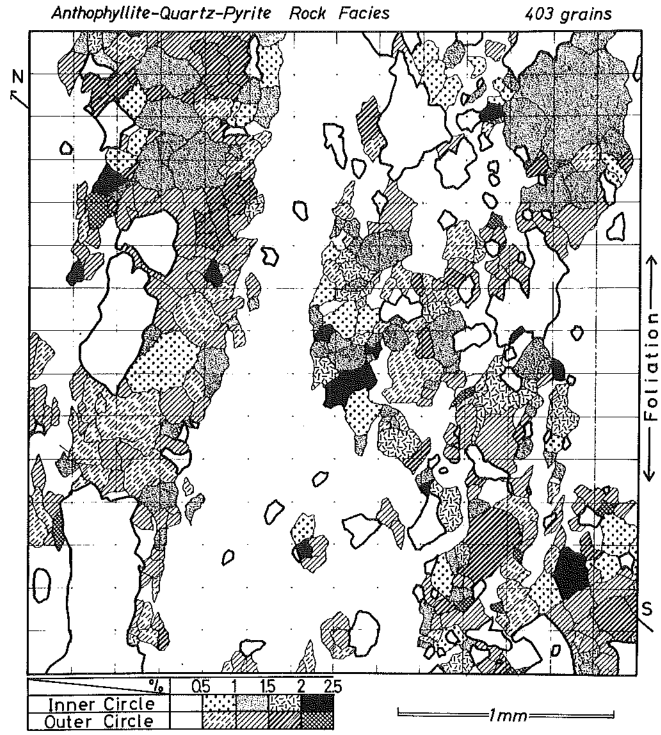

Fig. 11 A.V.A. detailed map of the squared area in Fig. 10.

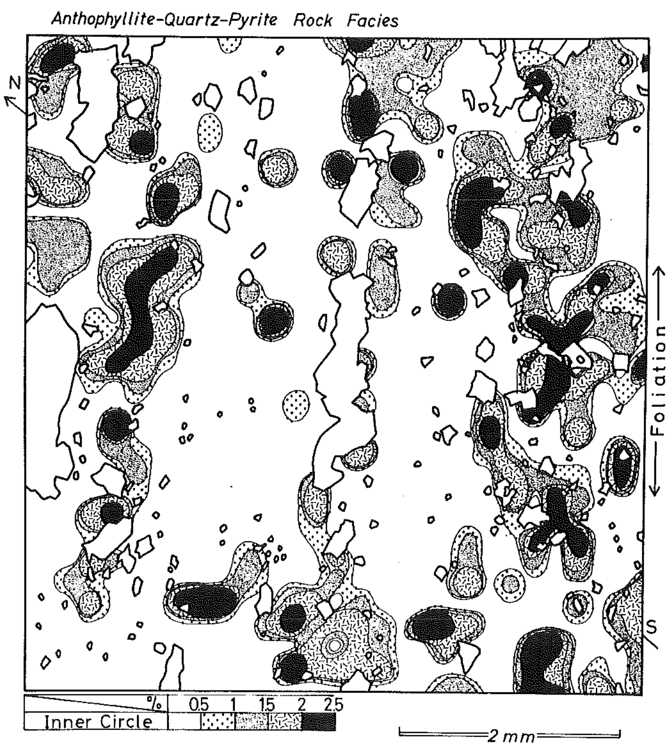

Fig. 12a A.V.A. Contour map belonging to inner circle of Fig. 9, which is maintained by making the statistical contour lines of concentration grade in respective group.

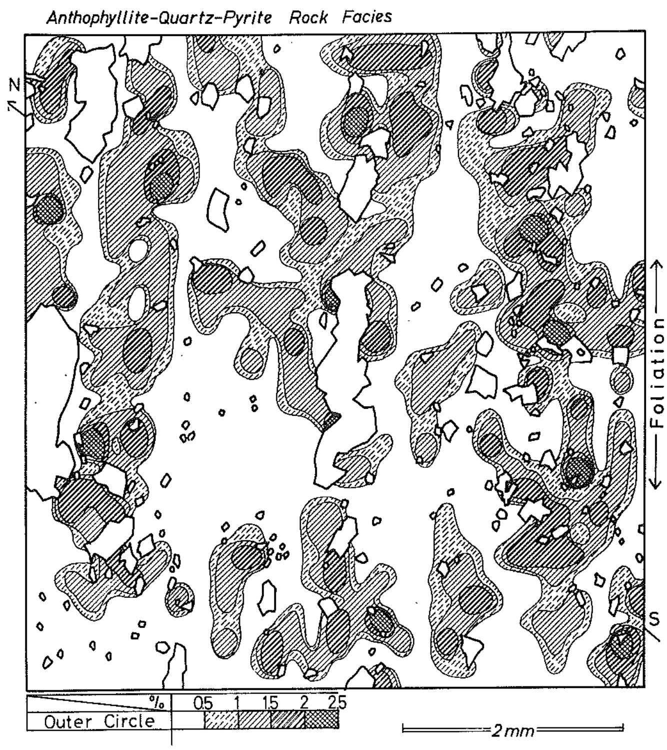

Fig. 12b A.V.A. Contour map belonging to outer circle of Fig. 9, which is maintained by making the statistical contour lines of concentration grade in respective group.

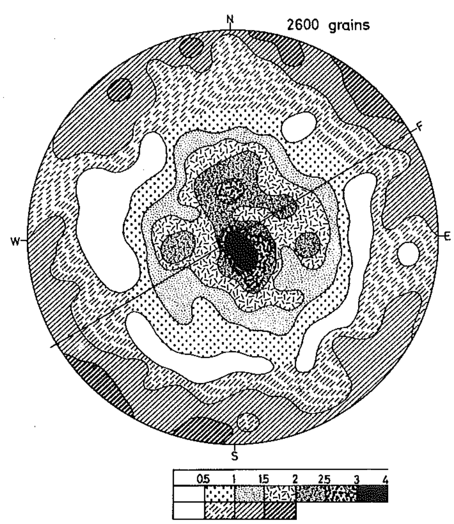

Fig. 13 A representative quartz fabric pattern of anthophyllite-cordierite-quartz-pyrite rock facies. The upper column is the concentration degree of the inner circle, the lower is one of the outer circle.

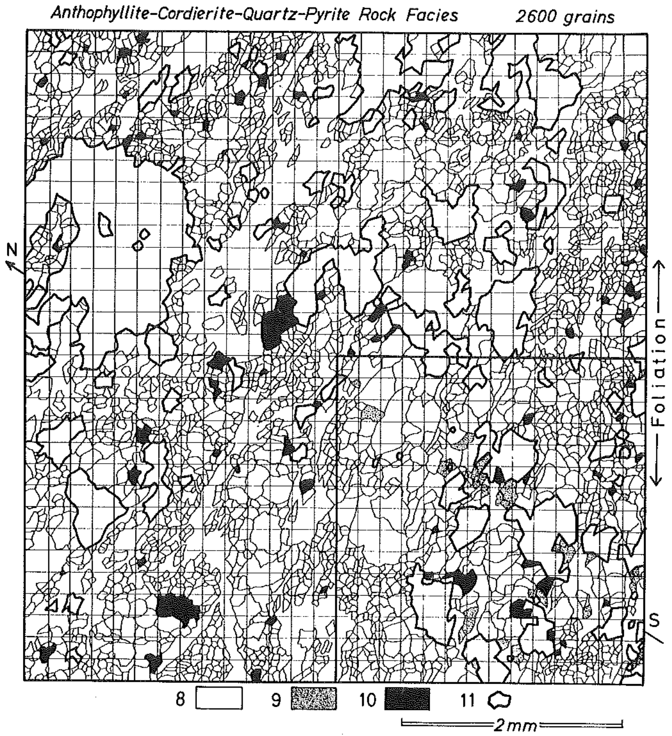

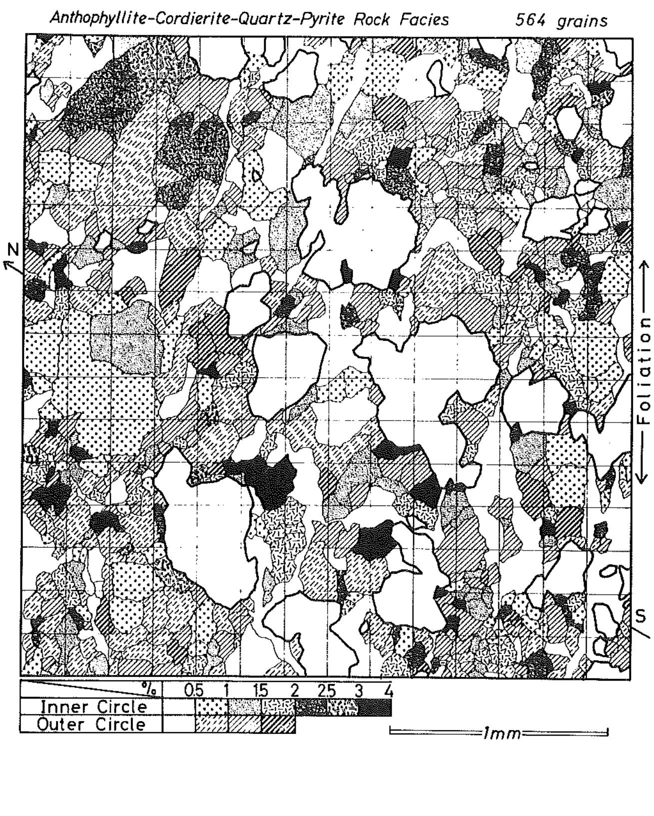

Fig. 14 A measured area in a thin section of anthophyllite- cordierite- quartz-pyrite rock facies for quartz fabric analysis. Furthermore, within a small squared area, the more detailed analyses as shown in Fig. 15 and Fig. 27 are carried out. The vacant matrix consists of plagioclase, biotite, sillimanite, perthite, chlorite and a small amount of corundum. 8: measured quartz grains with the definite coordination relation. 9: measured quartz grains without the definite coordination relation. 10: particularly, measured quartz grains plotted to the most concentrated central point of Fig. 13. 11: pyrite grains.

Fig. 15 A.V.A. detailed map of the squared area in Fig. 14.

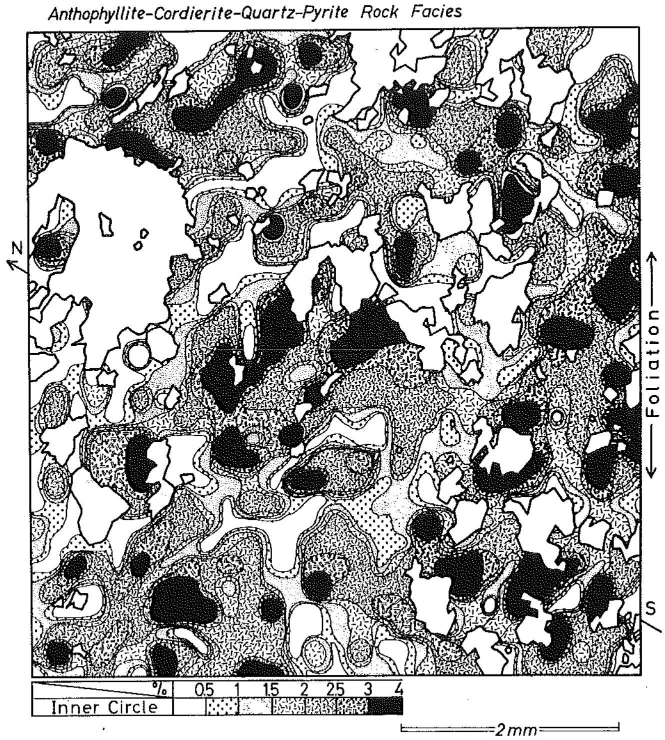

Fig. 16a A.V.A. Contour Map belonging to inner circle of Fig. 13, which is maintained by making the statistical contour lines of concentration grade in respective group.

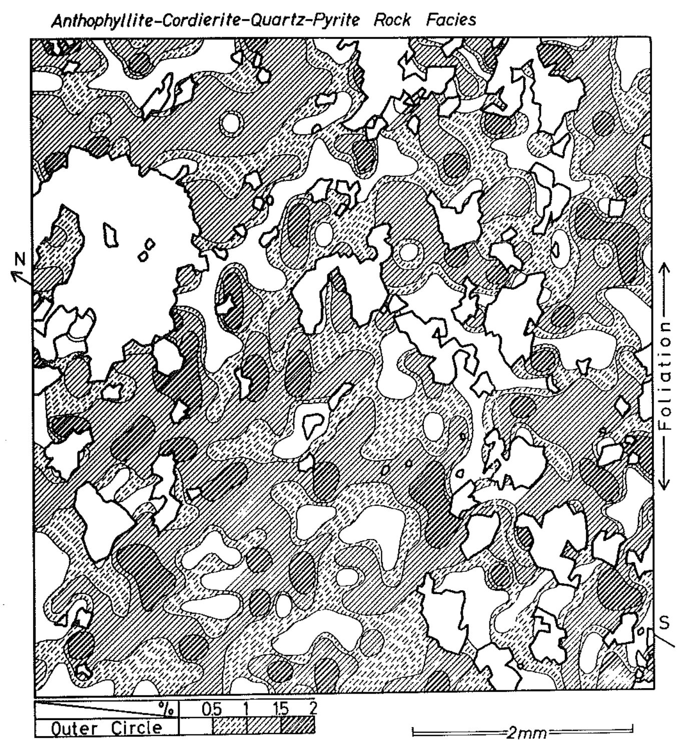

Fig. 16b A.V.A. Contour Map belonging to outer circle of Fig. 13, which is maintained by making the statistical contour lines of concentration grade in respective group.

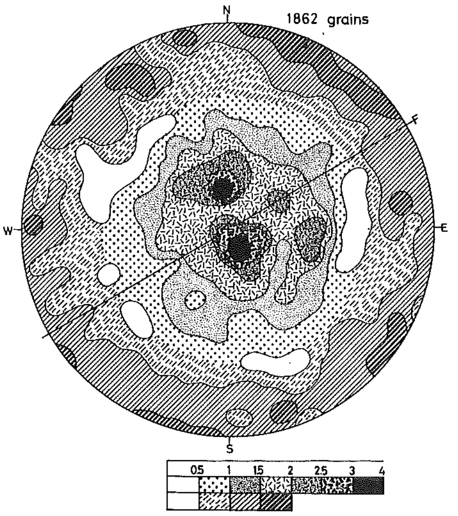

Fig. 17a Fabric pattern for fine-grained quartz facies without sulphide ore minerals in Fig. 13. The symbol marks correspond to those of Figs. 13, 16a and 16b.

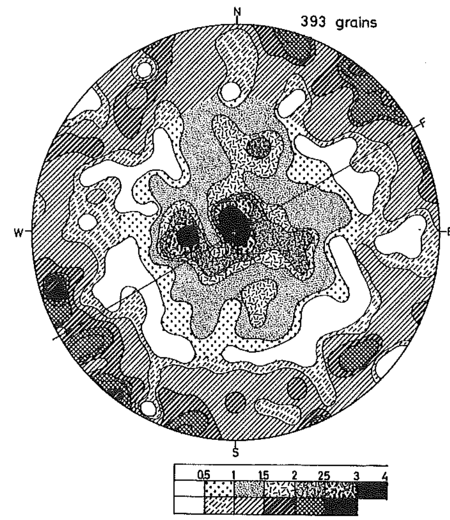

Fig. 17b Fabric pattern for fine-grained quartz facies with sulphide ore minerals in Fig. 13.

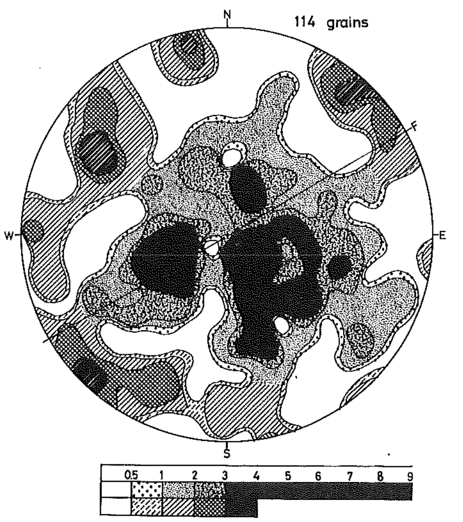

Fig. 17c Fabric pattern for coarse-grained quartz facies with sulphide ore minerals in Fig. 13.

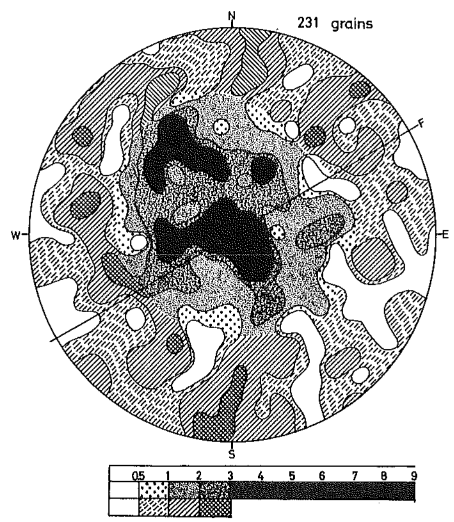

Fig. 17d Fabric pattern for coarse-grained quartz facies without sulphide ore minerals in Fig. 13.

Further studies on coordination of quartz

The writer has also examined the angle formed by c-axes of adjoining quartz grains.

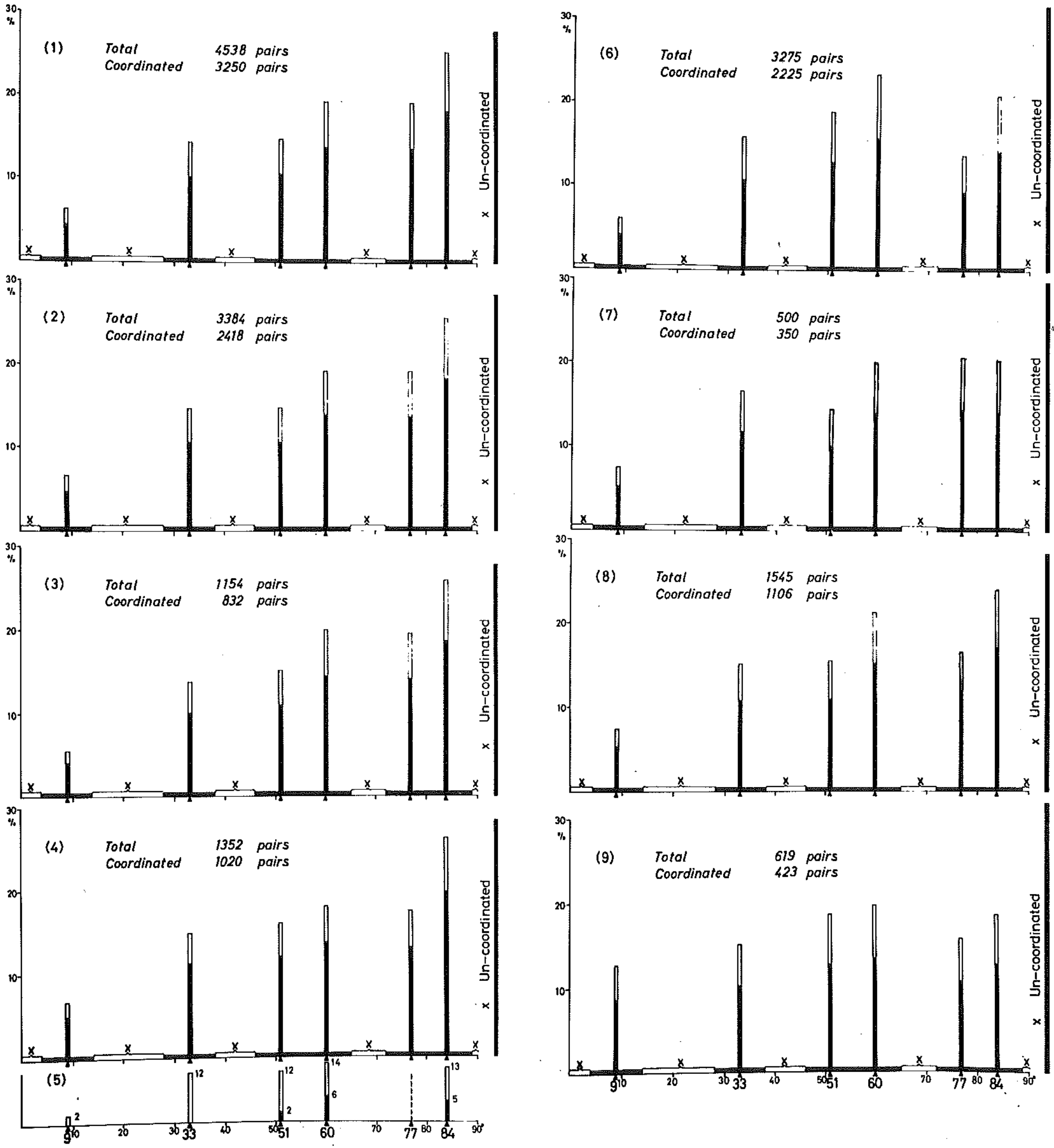

Fig. 18 Distribution and frequency diagrams for c-axis angle of the adjoining quartz grains in each rock facies.
(1) sericite-quartz-andalusite-pyrite rock facies
(2) quartz rich layer part in (1) facies
(3) sericite rich layer parts in (1) facies
(4) sericite-quartz-andalusite-pyrite rock facies

(5) theoretical values of modes and theoretical concentration frequency for three or four quartz grains after Japanese twin law
(6) anthophyllite-cordierite-quartz-pyrite rock facies
(7) anthophyllite-cordierite-quartz-pyrite rock facies
(8) cordierite-quartz-pyrite rock facies
(9) anthophyllite-quartz-pyrite rock facies

Cross mark is out of modes; un-coordinated. In frequency histograms drawn by the framed line, they are modes excluding un-coordination pairs. The solid line means modes including un-coordination pairs. In the case of (5), the framed line means the numbers of coordination for four grains and the solid line does those for three grains.

(1) *sericite-quartz-andalusite-pyrite rock facies:*

The number of measured pairs in each of these figures is 4538, 3384, 1154 and 1352 respectively. The results are as follows.

(a) The distribution of angles is not random, as several significant peaks occur on the frequency diagrams. Modes occur at 9°, 33°, 51°, 60°, 77° and 84° as shown in Figs. 18-(1), -(2), -(3) and -(4). The range of mode is taken as ±5° around each central value considering the measuring error. The method applied here is owing to the previous work (WATANABE, 1971). The degree of concentration at each mode except for 9° is very similar in the four diagrams. About three-quarters of the measured pairs plot at the modes.

In Fig. 18-(1),

mode including un-coordinated pairs	mode excluding un-coordinated pairs	central value of concentration
4.5%	6.3%	at 9°
10.3	14.4	33°
10.7	14.9	51°
13.9	19.4	60°
13.8	19.3	77°
18.4	25.7	84°
28.4		for un-coordination

In Fig. 18-(2),

mode including un-coordinated pairs	mode excluding un-coordinated pairs	central value of concentration
4.7%	6.6%	at 9°
10.6	14.6	33°
10.6	14.8	51°
13.7	19.2	60°
13.7	19.1	77°
18.4	25.7	84°
28.5		for un-coordination

In Fig. 18-(3),

mode including un-coordinated pairs	mode excluding un-coordinated pairs	central value of concentration
4.0%	5.5%	at 9°
10.0	13.8	33°
10.9	15.1	51°
14.4	20.0	60°
14.1	19.6	77°
18.7	26.0	84°
27.9		for un-coordination

In Fig. 18-(4),

mode including un-coordinated pairs	mode excluding un-coordinated pairs	central value of concentration
5.1%	6.8%	at 9°
11.3	15.0	33°
12.1	16.1	51°
13.8	18.2	60°
13.2	17.6	77°
19.9	26.4	84°
28.4		for un-coordination

The writer proposes the term "coordination relation" for the arrangement of the 71–72% of measured pairs which are in special crystallographic relationships and "un-coordination relation" for the remaining 28–29%.

(b) Fig. 19a to 19g. The planes of great circle formed by the *c*-axes of two adjoining quartz grains have a rather special distribution. Most of the planes of great circle of 500 pairs chosen by random selection from the 4538 pairs, as shown in Fig. 19a, are arranged near to the outer circle as defined in Fig. 1. When a grain from the central maximum is involved, the plane of great circle always has a "bridge relationship" joining this grain to one in the outer circle. Further analysis of this relationship was carried out by preparing "peak girdle diagrams"(WATANABE, 1971) on each concentration angle at 84°, 77°, 60°, 51°, 33° and 9°. The results are given in Fig. 19b to 19g. They have the following main features: (i) planes of great circle formed by *c*-axes of two adjoining grains are not only lying in the outer circle, but also form "bridge relationship" between the grains plotted to the highest concentration area of the central maximum and those of the outer circle. (ii) Moreover, the bridge relationship between the grains plotted to the highest concentration area of the central maximum and those of outer circle are limited to high angle. This is especially noticeable in the 84° diagram.

These grains belonging to the mode at 84° may be Japanese twin crystals, though it is microscopically impossible to identify the composition plane between them, because the twinned crystals of quartz in which the composition plane is $\xi(11\bar{2}2)$ and the *c*-axes cross at an angle of 84°33′ are usually known as "Japanese twin". The twin planes, in this meaning, of 837 pairs belonging to the mode at 84° have been plotted in Fig. 20.

The Japanese twin crystal from Narushima, Nagasaki Pref., Japan and its angular relationships are presented in Fig. 21.

Judging from Fig. 20, most of the planes of Japanese twin are concentrated in a narrow ring with radius of about 42° around the centre of the diagram. The centre is the highest concentration point corresponding to the inclination of the shoot of ore bodies, as shown in Fig. 1. This means that there is very commonly a Japanese twin relation between one quartz grain belonging to the centre of diagram and one in the outer circle. In addition the same twin relationship frequently occurs between two grains in the outer circle as indicated by the presence of a number of twin-planes nearly perpendicular to the perimeter of the diagram in Fig. 20.

(c) Fig. 22 covers the same thin slip area as Fig. 3 and shows the distribution of *c*-axis coordination in terms of the six modes of coordination.

(2) *cordierite-quartz-pyrite rock facies:*

The number of measured pairs is 1545. The results are as follows.

(a) Peaks are again revealed at 9°, 33°, 51°, 60°, 77° and 84° on the distribution frequency diagram. The degree of concentration for each mode is very similar as shown in Fig. 18-(8). About three-quarters of all measured pairs

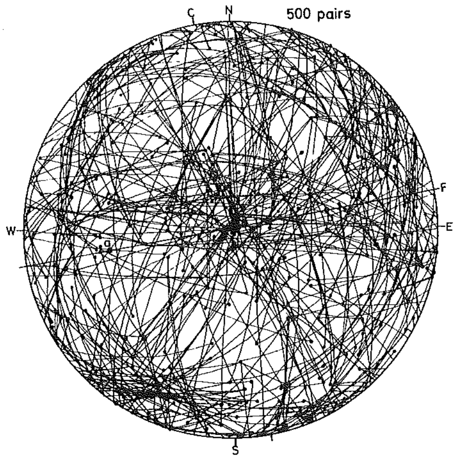

Fig. 19a Peak girdle of 500 pairs of c-axis angles of the adjoining quartz grains of sericite-quartz-andalusite-pyrite rock facies.

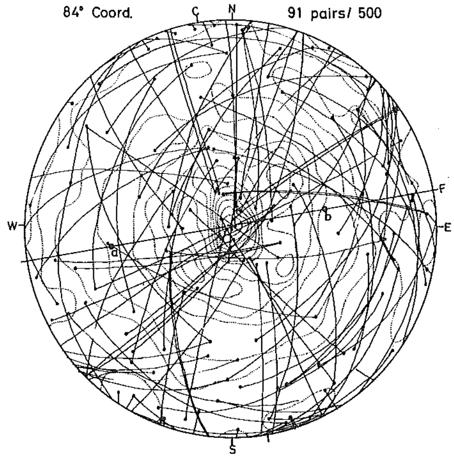

Fig. 19b Peak girdle at 84° peak.

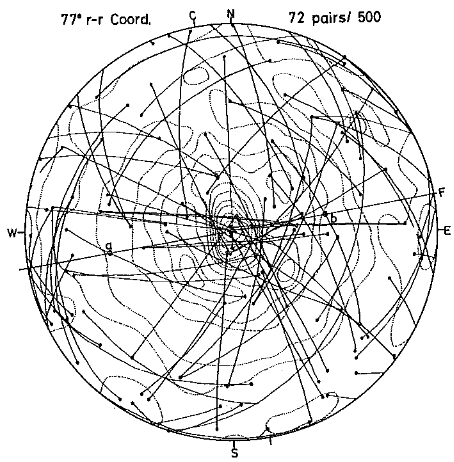

Fig. 19c Peak girdle at 77° peak.

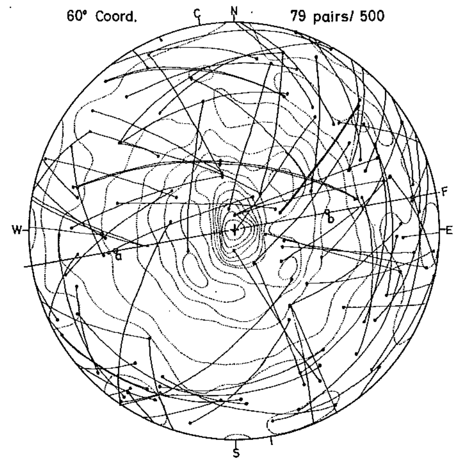

Fig. 19d Peak girdle at 60° peak.

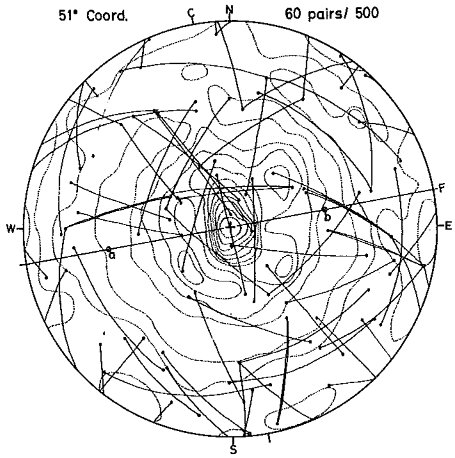

Fig. 19e Peak girdle at 51° peak.

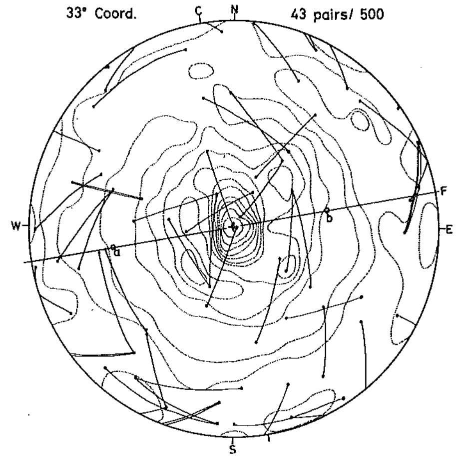

Fig. 19f Peak girdle at 33° peak.

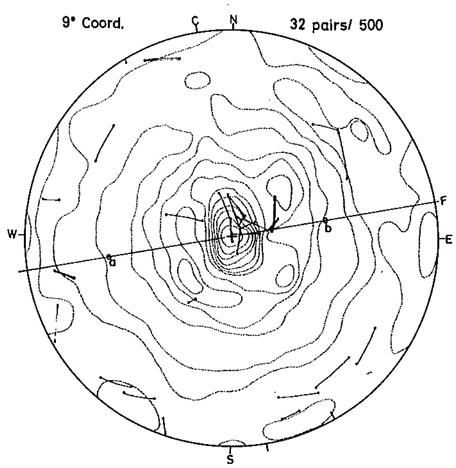

Fig. 19g Peak girdle at 9° peak.

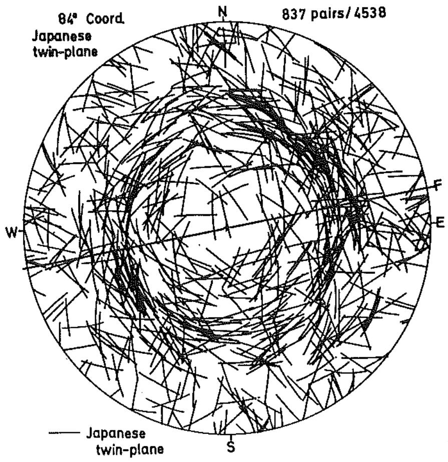

Fig. 20 A representative diagram demonstrated dispositions of Japanese twin-planes in sericite-quartz-andalusite-pyrite rock facies.

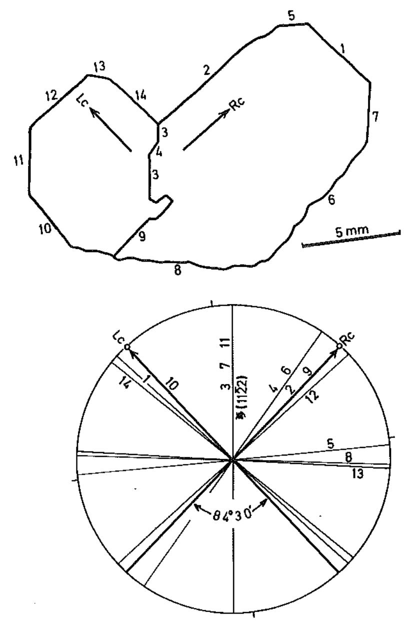

Fig. 21 Natural crystal showing the Japanese twin relation, from Narushima, Nagasaki Pref., Japan and its measured stereographic projection. The denominating numbers mean the natural crystal faces respectively. Rc and Lc denote respectively *c*-axis of right and left half parts of crystal.

Fig. 22 Distribution Map of c-axis coordination on each concentration angle in sericite-quartz-andalusite-pyrite rock facies.
1: at 9°. 2: at 33°. 3: at 51°. 4: at 60°. 5: at 77°. 6: at 84°. 7: un-coordination relation. 8: measured quartz grains with the definite coordination relation. 9: measured quartz grains without the definite coordination relation.

are concentrated in the modes.
In Fig. 18-(8),

mode including un-coordinated pairs	mode excluding un-coordinated pairs	central value of concentration
5.3%	7.4%	at 9°
10.9	15.2	33°
11.1	15.6	51°
15.2	21.3	60°
11.9	16.6	77°
17.2	24.0	84°
28.4		for un-coordination

(b) Planes of great circle containing the *c*-axes of two adjoining quartz grains were plotted for each concentration mode and found to be quite similar to those obtained in the sericite-quartz-andalusite-pyrite rock facies. The figures for the 84° and 77° modes are reproduced (Figs. 23a and 23c) together with the plots of twin plane for the same data (Figs. 23b and 23d). The bridge relationship and the twin-plane pattern at 84° is virtually the same as that found in the sericite-quartz-andalusite-pyrite rock facies. The pattern of the 77° mode resembles that of 84°. Again most of the adjoining quartz grains belonging to coordination of 77° show a bridge relationship between one grain belonging to central maximum and one in the outer circle. Although the degree of concentration in the 77° mode is rather high and the features as shown in Figs. 23c and 23d resemble those of Japanese twinning, it can not be interpreted in terms of a Japanese twin relationship. Crystallographically, the *c*-axial angle of 77° is acquired when two quartz grains adjoin so as to have common r($10\bar{1}1$) between them, because the axial angle between the *c*-axis and r-plane is precisely 38° 13′. This must, therefore, be interpreted as Estérel twinning, though it is proposed to refer to it in the present paper as the "r-r coordination relation". Fig. 24 covers the same area of thin section as Fig. 6 and is a distribution map of *c*-axis coordination in terms of the six modes of coordination.

(3) *anthophyllite-quartz-pyrite rock facies:*

The number of measured pairs is 619. The results are as follows.

(a) Peaks again occur on the distribution frequency diagram at 9°, 33°, 51°, 60°, 77° and 84°. The degree of concentration for each mode is very similar to that found in previous facies (Fig. 18-(9)). About two-thirds of all measured pairs are concentrated in the modes.

In Fig. 18-(9),

mode including un-coordinated pairs	mode excluding un-coordinated pairs	central value of concentration
8.6%	12.6%	at 9°
10.2	15.0	33°
12.6	18.5	51°
13.4	19.7	60°
10.7	15.7	77°
12.6	18.5	84°
31.7		for un-coordination

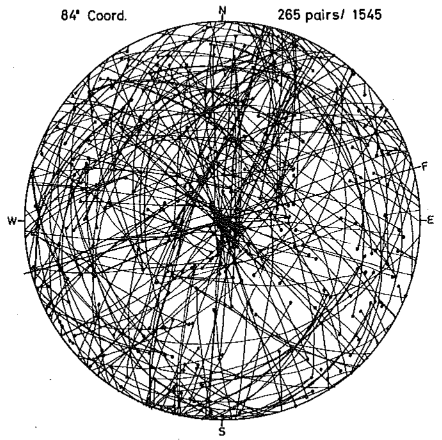

Fig. 23a Peak girdle at 84° peak in cordierite-quartz-pyrite rock facies

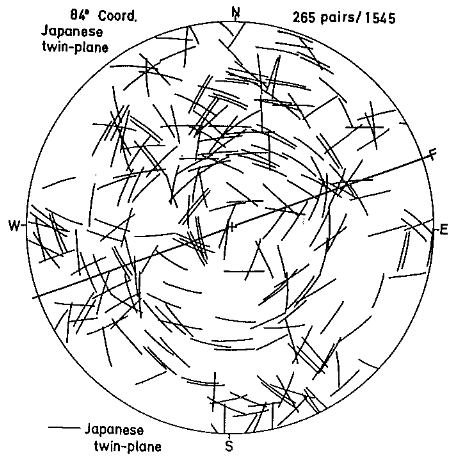

Fig. 23b A. diagram demonstrated dispositions of Japanese twin-planes from Fig. 23a.

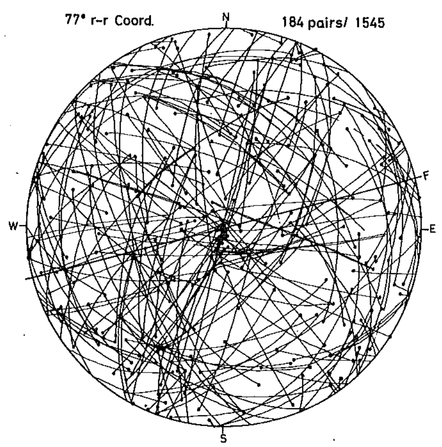

Fig. 23c Peak girdle at 77° peak in cordierite-quartz-pyrite rock facies

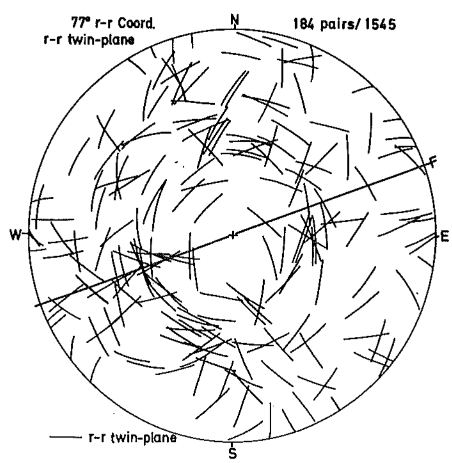

Fig. 23d A diagram demonstrated dispositions of Estérel twin-planes from Fig. 23c.

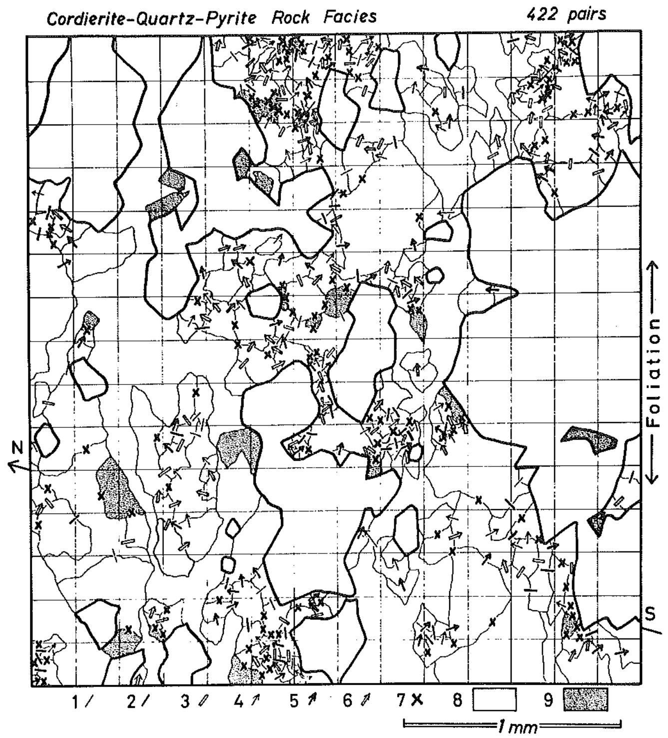

Fig. 24 Distribution Map of *c*-axis coordination on each concentration angle of the squared area in Fig. 6.
1: at 9°. 2: at 33°. 3: at 51°. 4: at 60°. 5: at 77°. 6: at 84°. 7: un-coordination relation. 8: measured quartz grains with the definite coordination relation. 9: measured quartz grains without the definite coordination relation.

(b) Plots of the traces of planes of great circle containing the *c*-axes of two adjoining quartz grains were checked for each concentration mode. The diagrams are very similar to those obtained in previous facies both in terms of the bridge relationships of Japanese twins and of the r-r coordination relations. Fig. 25 which covers the same area of thin section as Fig. 10 shows the distribution of *c*-axis coordination in terms of the six modes of coordination.
(4) *anthophyllite-cordierite-quartz-pyrite rock facies:*

Two samples were analysed. The number of measured pairs is 3275 and 500 respectively. The results are as follows.
(a) Peaks are again found at 9°, 33°, 51°, 60°, 77° and 84° on the distribution frequency diagram. The degree of concentration for each mode is very similar to those of previous facies as shown in Figs. 18-(6) and 18-(7). About two-thirds of measured pairs are concentrated in the modes.

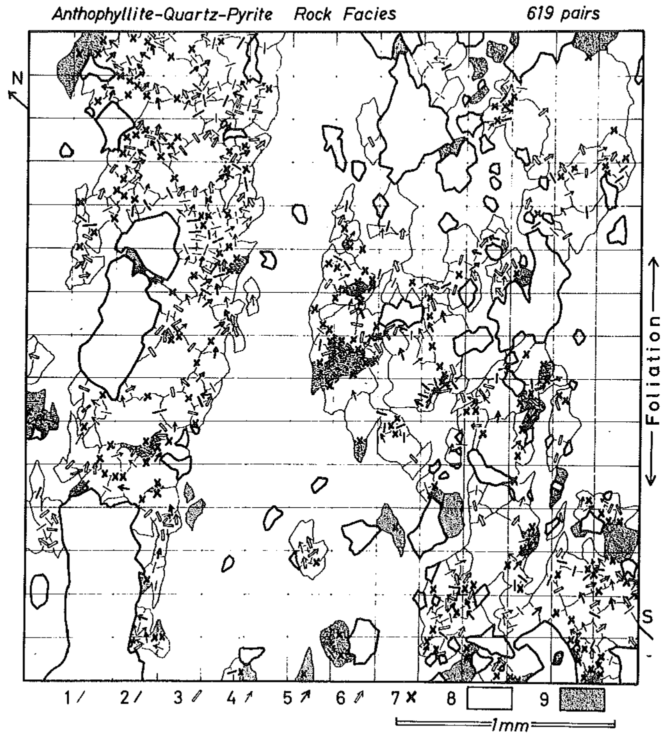

Fig. 25 Distribution Map of *c*-axis coordination on each concentration angle of the squared area in Fig. 10.
1: at 9°. 2: at 33°. 3: at 51°. 4: at 60°. 5: at 77°. 6: at 84°. 7: un-coordination relation. 8: measured quartz grains with the definite coordination relation. 9: measured quartz grains without the definite coordination relation.

In Fig. 18-(6),

mode including un-coordinated pairs	mode excluding un-coordinated pairs	central value of concentration
4.2%	6.1%	at. 9°
10.8	16.0	33°
13.0	19.1	51°
16.0	23.6	60°
9.5	14.0	77°
14.4	21.2	84°
32.1		for un-coordination

In Fig. 18-(7),

mode including un-coordinated pairs	mode excluding un-coordinated pairs	central value of concentration
5.2%	7.4%	at 9°
11.6	16.6	33°
10.2	14.6	51°
14.2	20.3	60°
14.6	20.9	77°
14.2	20.3	84°
30.0		for un-coordination

(b) Plots of the traces of planes of great circle containing the *c*-axes of two adjoining quartz grains have been made for each concentration mode. These diagrams are essentially identical to those obtained for previous facies.

The bridge relationships and the pattern of twin-planes for the 84° mode (Figs. 26a and 26b) are entirely analogous to those presented in previous facies. The principal features of r-r coordination are likewise very similar to those of previous facies. Fig. 27 which covers the same area of thin section as Fig. 14 shows the distribution of *c*-axis coordination in terms of the six modes of coordination.

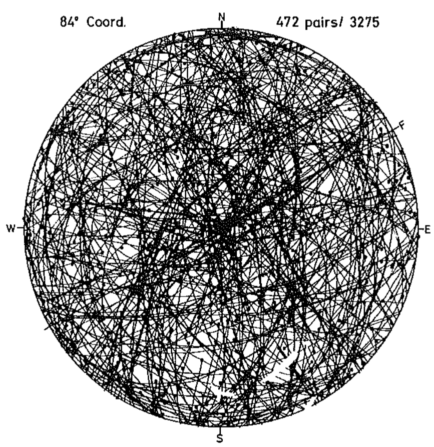

Fig. 26a Peak girdle at 84° peak in anthophyllite-cordierite-quartz-pyrite rock facies

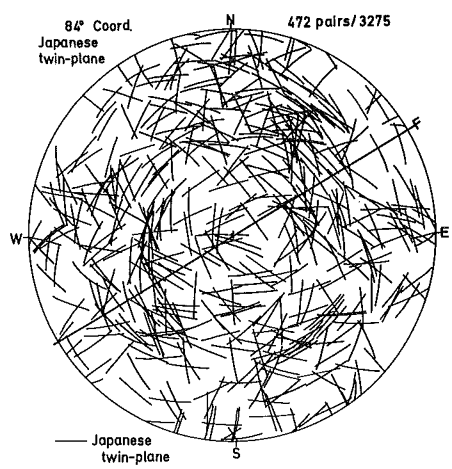

Fig. 26b A diagram demonstrated dispositions of Japanese twin-planes from Fig. 26a.

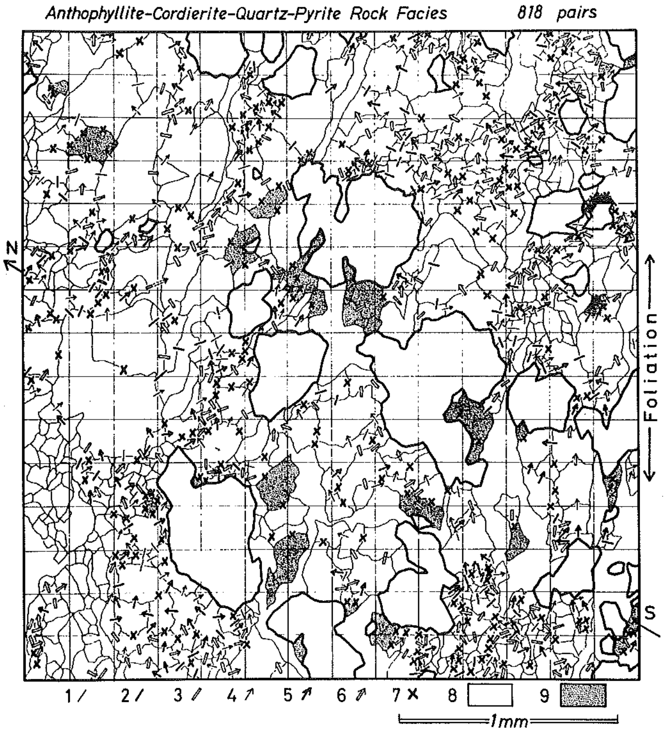

Fig. 27 Distribution Map of c-axis coordination on each concentration angle of the squared area in Fig. 14.
1: at 9°. 2: at 33°. 3: at 51°. 4: at 60°. 5: at 77°. 6: at 84°. 7: un-coordination relation. 8: measured quartz grains with the definite coordination relation. 9: measured quartz grains without the definite coordination relation.

Crystallographical consideration on c-axis coordinations of Japanese and Estérel twinning

The writer has previously (1971) attempted to explain the observed modes at 84°, 77°, 60°, 51°, 33° and 9° on the basis of multiple twinning on just one or two twin laws, and has arrived at the following conclusions:-

"For the existence of such definite modes in the statistical treatment of c-axis angles and their spatial disposition, some crystallographical considerations may serve as an available interpretation on their mutual relationships. When A and B grains of quartz adjoined side by side in the relation after Japanese twin law holding their $\xi(11\bar{2}2)$ in common, the c-axis of A and that of B grains takes the angle of 84°33′. In the case of third grain C adjoined to A and B grains and coordinated with B grain in a Japanese twin relation, the axial angle $\widehat{AC}$ may theoretically take the value of 60°54′. If the fourth grain D coordinated to the aggregation of A-B-C in a similar relation, the axial angles $\widehat{DA}$, $\widehat{DB}$ and $\widehat{DC}$ may respectively take 33°, 51° and 60°".

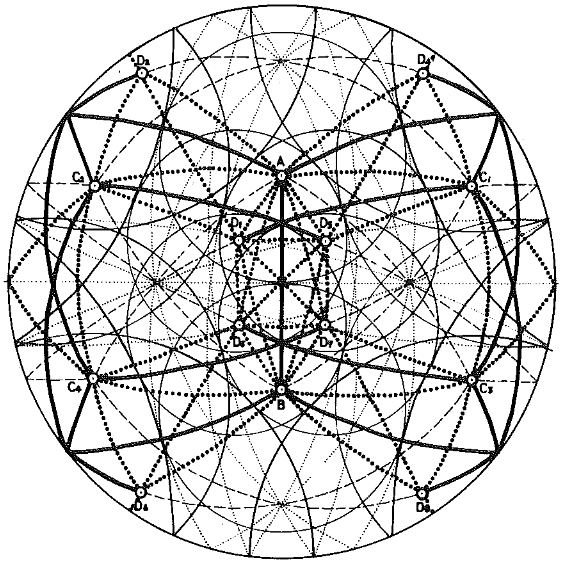

Fig. 28 Crystallographical relation of coordination after Japanese twin law for grains A, B, C and D.

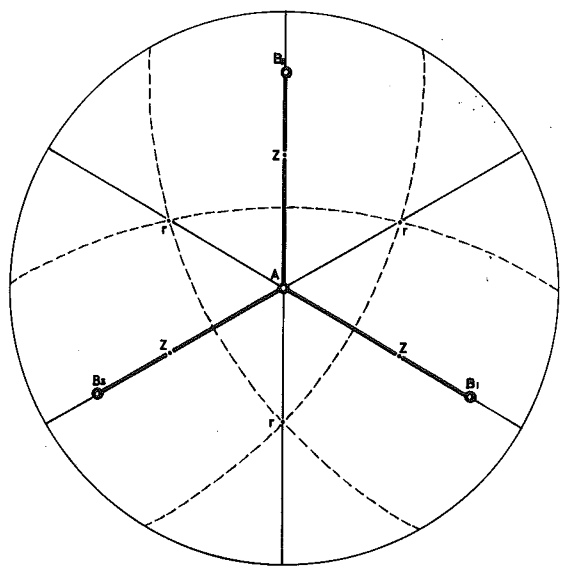

Fig. 29 Crystallographical relation of coordination by r(10$\bar{1}$1).

These relationships are presented in stereographic projection (Fig. 28).

"The statistical concentration of examined axial angles to those modes of 84°, 60°, 51° and 33° is well understood as the result of coordination effect of each grain after Japanese twin law. The statistically obtained values as modes in grain orientation relation are satisfactorily in agreement with the theoretical values in crystallography. The theoretical concentration frequency for each angle of *c*-axis coordination for three quartz grains is given as follows. Five sets at 84°, 6 sets at 60° and 2 sets at 51°. At the same time, the theoretical concentration frequency for each angle of *c*-axis coordination for four quartz grains is respectively given as follows. Thirteen sets at 84°, 14 sets at 60°, 12 sets at 51°, 12 sets at 33° and 2 sets at 9°. As a result, the ratio in the theoretical concentration frequency for 84°, 60°, 51° and 33° of *c*-axis coordination for three or four quartz grains is generally given as 1:1:1:1. Actually, this theoretical result is very well accordant with the result of examined ratios".

Theoretical values of modes and theoretical concentration frequency for each angle of *c*-axis coordination for three or four quartz grains after the Japanese twin law are given in Fig. 18-(5) based on Fig. 28.

In Fig. 28, the thick solid line shows the *c*-axis angle of 84°, the fine dotted line is $\xi(11\bar{2}2)$: Japanese twin-plane (composition plane), the broken line is the supplement of the *c*-axis angle of Japanese twinning: 96° the thick dotted line is the coordinating angle which is theoretically estimated as the result of three or four grains coordinations, and the fine solid line is representing a circle of 42° in radius as a half the number of 84° around a grain.

When two grains (A and B) are in Japanese twin relationships with $\xi(11\bar{2}2)$ in common, their *c*-axes are at an angle of 84°33′. In the case of a third grain (c) joined to A and B and coordinated with B in Japanese twin relation, the axial angles $A\hat{}C_1$ or $A\hat{}C_2$ may theoretically take the value of 60°54′. If C and A are in twin relationships, the axial angles $B\hat{}C_3$ or $B\hat{}C_4$ will again be 60°54′. The axial angles $C_1\hat{}C_3$ or $C_2\hat{}C_4$ will be 51° and the axial angles $C_1\hat{}C_2$ or $C_3\hat{}C_4$ 60°.Thus, a twin triplet (A-B-C) gives 5 sets of angles at 84°, 6 sets at 60° and 2 sets at 51° as shown in Fig. 18-(5).

If a fourth grain(D) is joined to A, B and C also in twin relationships, the following angles may occur: $C_1\hat{}D_1$, $C_2\hat{}D_3$, $C_3\hat{}D_5$, $C_4\hat{}D_7$, $C_1\hat{}D_2$ $C_3\hat{}D_6$, $C_2\hat{}D_4$ or $C_4\hat{}D_8$ all 84°, $D_1\hat{}D_2$, $D_3\hat{}D_4$, $D_5\hat{}D_6$, $D_7\hat{}D_8$, $D_1\hat{}B$, $D_3\hat{}B$, $D_5\hat{}A$ or $D_7\hat{}A$ all 60°, $C_1\hat{}D_3$, $C_3\hat{}D_7$, $C_2\hat{}D_1$, $C_4\hat{}D_5$, $D_1\hat{}D_7$, $D_3\hat{}D_5$, $D_2\hat{}A$, $D_4\hat{}A$, $D_6\hat{}B$ or $D_8\hat{}B$ all 51°, $C_1\hat{}D_4$, $C_2\hat{}D_2$, $C_3\hat{}D_8$, $C_4\hat{}D_6$, $D_1\hat{}A$, $D_3\hat{}A$, $D_5\hat{}B$, $D_7\hat{}B$, $D_1\hat{}D_3$, $D_1\hat{}D_5$, $D_3\hat{}D_7$ or $D_5\hat{}D_7$ all 33°, and $D_2\hat{}D_8$ or $D_4\hat{}D_6$ both 9°. Respectively, C_1, C_2, C_3 and C_4, and D_1, D_2, D_3 D_4 D_5, D_6, D_7 and D_8 signify C and D grains at the dispositions which are controlled by their trigonal axes.

The final possible total for a triplet and a four component twin (A-B-C-D) is therefore 13 sets of angles at 84°, 14 sets at 60°, 12 sets at 51°, 12 sets at 33° and 2 sets at 9° as shown in Fig. 18-(5).

The degree of concentration at mode of 77° is rather high on the frequency distribution diagram. This can never be produced by Japanese twin relationships. In a previous paper the writer described that the pairs having axial angle of 77°, in the biotite banded genisses of the Nishidohira basement complex, are concentrated in the neighbourhood of the biotite layers and scarce in the leucocratic layers composed of plagioclase and quartz. However, no relationships of this type is found in the present study. There is, for example, no difference in the degree of concentration of the mode of 77° between the quartz rich layer and sericite rich layer in sericite-quartz-andalusite-pyrite rock facies, as shown in Figs. 18-(1), 18-(2) and 18-(3).

Crystallographically, the axial angle of 77° is acquired when the two quartz grains adjoin so as to have r$(10\bar{1}1)$ as a common plane. The relationships is represented in stereographic projection in Fig. 29. The grain (A) can develope a twin of this type coordinating with the grain (B) at three points around its trigonal axis. They will have r$(10\bar{1}1)$ or z$(10\bar{1}1)$ as the common plane and axial angle $\widehat{AB}$ 76°26′ because the angle between *c*-axial direction [0001] and $(10\bar{1}1)$ of single grain, viz. m$(10\bar{1}0)^r(10\bar{1}1)$ is 38° 13′

This coordinated relation, therefore, is interpreted as a twin after Estérel law being twin plane of $(10\bar{1}1)$ and *c*-axial angle of 76°26′ between two β-quartz grains.

Interpreting quartz fabric analyses in terms of twinning

All of the above-mentioned facies gave patterns characteristic of duplicate spheroidal symmetry with a few additional sub-maxima on a small circle with radius of 25° to 26° around the main maximum point. The main maximum corresponds to the plunge of the shoot of ore bodies. Further, on the basis of prior knowledge of the effect of Japanese and Estérel twinning, analytical studies were made in the hope of being able to account for the quartz fabric patterns in terms of twinning. The following may indicate the main factors controlling the formation of those patterns.

a) Twin after Japanese law is the main coordination for the association of the grains.

b) Most great circles formed by *c*-axes of two adjoining quartz grains are in "bridge relationships". This relationship is especially conspicuous for the angle of 84°. Assuming that the feature is due to the presence of Japanese twinning, Figs. 20, 23b, and 26b show the distribution of Japanese twin-planes. It will be seen that most of these twin-planes are concentrated on a circle with radius of 40° centred on the centre of the diagram while the rest lie close to the perimeter of the diagram and are perpendicular to it.

This is considered to be confirmation of the existence of twinning triplets. When triplets exist more than one orientation is possible:- (i) Fig. 30 represents the coordination relations for three grain associations. When a twin triplet A-B-C exists as shown in Fig. 28, $\hat{AB}$, $\hat{BC}$ and $\hat{AC}$ being *c*-axial angles of adjoining grains are respectively 84°, 84° and 60°. The Japanese twin-plane $\xi(11\bar{2}2)$ is at the exactly middle point between grain A and B, and grain B and C. If the coordination relation for these three grains is rotated to shift to the position A-B_1-C_1 or A-B_2-C_2 and so on, the twin-plane describes a circular path of the type observed in Fig. 20 which suggests that each coordination relation has a rotational relation around the central grain A, so that the path of the twin-plane is a circle with radius of 42° around grain A. A served set of twin-planes lies in the outer circle perpendicular to the perimeter. (ii) Fig. 30 also shows another possible coordination relations for a three grains association (b-A-c). When the triplet has a relationship as shown in Fig. 28, $\hat{bA}$, $\hat{Ac}$ and $\hat{bc}$ being *c*-axial angles of adjoining grains are respectively 84°, 84° and 60°. In this case, the Japanese twin-plane $\xi(11\bar{2}2)$ is never perpendicular to the perimeter. It is always at the exactly middle point between grain A and b, and grain A and c. Accordingly, a rotational shift in the direction of b_1-A-c_1, b_2-A-c_2 and so on, causes the two twin-planes to describe a common path a circle with radius of 42° around grain A. It is, thus, reasonable that the concentration of twin-planes at 42° from the central point is twice as great for twin triplets of the type A-b-c as it is for twin triplets of the type A-B-C. In both cases the highest concentration of *c*-axes of quartz grains is at the central position (grain A).

The fabric patterns obtained from each facies in the zone of alteration can thus readily be interpreted in terms of arrangement and degree of development of Japanese twinning. The same conclusion was reached previously concerning fabric patterns obtained from the Nishidohira biotite gneiss complex (WATANABE, 1971). A representative pattern of the Nishidohira biotite gneiss complex which is interpreted as a case of triplet twinning after the Japanese law is shown in Fig. 31. In this case, however, one grain in each association plots not in a centre of the pattern, but on an inner circle of it.

Coordination between quartz and pyrite

Sulphide minerals (especially pyrite) are present in all mineralized zones and can constitute several tens of percentages of the total rock. Rocks containing pyrite together with silicate minerals such as quartz, plagioclase, biotite, sericite, cordierite, anthophyllite, andalusite, fuchsite, sillimanite, chlorite etc, sometimes constitute an early phase prior to the major period of

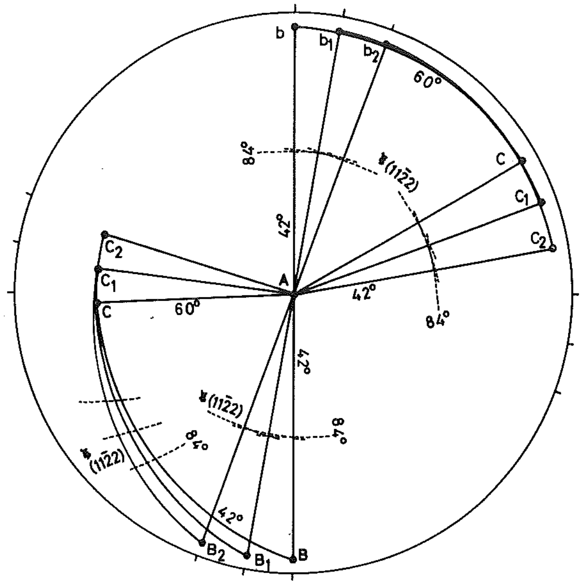

Fig. 30 A diagrammatical projection of three grains coordination after Japanese twin relation in these alteration rocks.

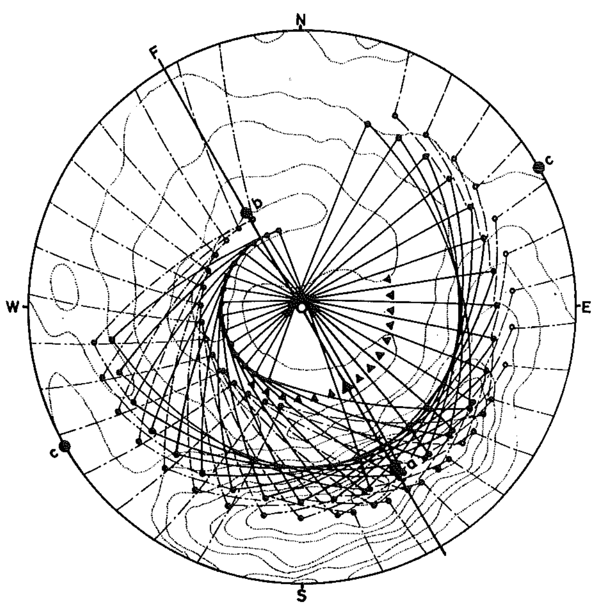

Fig. 31 Theoretical projection of three grains coordination after Japanese twin relation in the case of the Nishidohira gneiss complex (J. WATANABE, 1971).

ore deposition.

In cases where the quartz coordinations have been studied, it may be important to know whether the orientation of pyrite grains has been affected by the fixed coordinations known to exist among quartz grains. For this reason, pyrite grains from Figs. 2, 6, 10 and 14 have been studied. Orientation of a-axes of pyrite grains, estimated from two edges of the cube form, has been determined in thin section with the help of a universal stage and an oblique and/or vertical illuminator. Patterns obtained from each thin section are shown in Fig. 32-(1) to Fig. 32-(4) respectively. A solid circle indicates the position of each measured a-axis and two open circles indicate the calculated positions of the other two axes. Pyrite fabric patterns from workable pyrite ore bodies at the 450 metre level of the Fudotaki ore bodies, located in a mineralized zone far to the east, are shown in Fig. 33-(1) to Fig. 33-(3) for comparison. It is obvious in every facies that most of the measured pyrite grains show strong preferred orientation with one a-axis plotting in the central area of the pattern, which corresponds to the inclination of the shoot of the ore bodies and the other two axes (calculated from the measured axis) plotting around the perimeter of the pattern. These patterns in fact bear a strong resemblance to the quartz patterns as shown in Figs. 1, 5, 9 and 13. This suggests that there may be a fixed crystallographic relationship between pyrite and quartz grains, accordingly, crystallographical studies were initiated in a search for special relationships between adjoined grains of quartz and pyrite. A histogram of registered angles between pyrite a-axis and quartz *c*-axis in adjoining grains shows maxima at 38°, 26°, (19–21°), 12° and 0° as shown in Fig. 34.

Though pyritohedral faces are seldom well developed, the existence of these maxima suggests that this form plays a major role in controlling the oriented growth of these two minerals, as shown in Fig. 35. In this figure, a pair of pyrite crystals with pyritohedral and cube faces twinned each other in twin axes [110] and [1$\bar{1}$0], viz. on the Iron Cross Law is projected on Wulff's net. Faces marked by a cross signify one twin individual and those marked by an open circle the other. If r(10$\bar{1}$1) of a quartz crystal is attached to the pyritohedral face e(0$\bar{1}$2) in such a way that the vertical plane which includes the *c*-axis of the quartz grain is perpendicular to the striation on the pyritohedral face, then two orientations of quartz are possible. In the first case the *c*-axis of the quartz grain lies parallel to the pole of another pyritohedral face (012) and plots on the stereogram 26° from the pole of (001). In the second case it plots 12° from the pole of (0$\bar{1}$0). The two orientations are shown schematically in the right corner of Fig. 35. If r(10$\bar{1}$1) is attached to a pyritohedral face e(0$\bar{1}$2) in such a way that the vertical plane including the *c*-axis is parallel to the striation direction on that pyritohedral face, then the

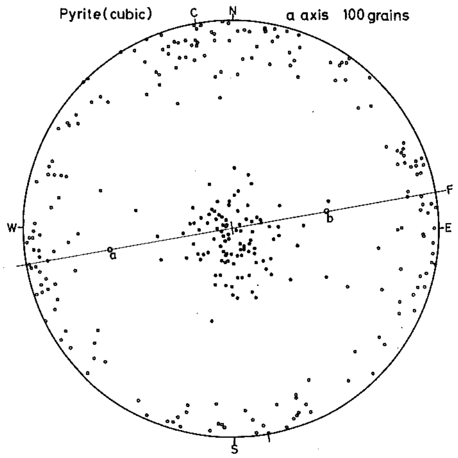

Fig. 32-(1) Pyrite fabric pattern of sericite-quartz-andalusite-pyrite rock facies.

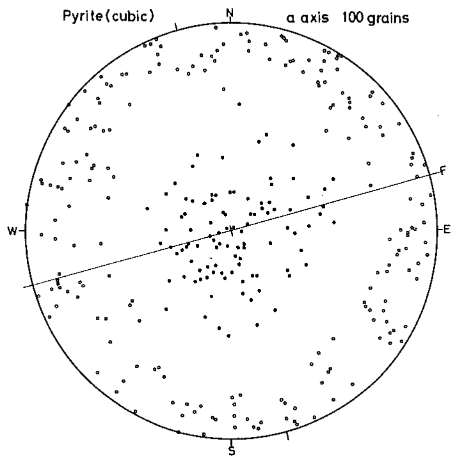

Fig. 32-(2) Pyrite fabric pattern of cordierite-quartz-pyrite rock facies.

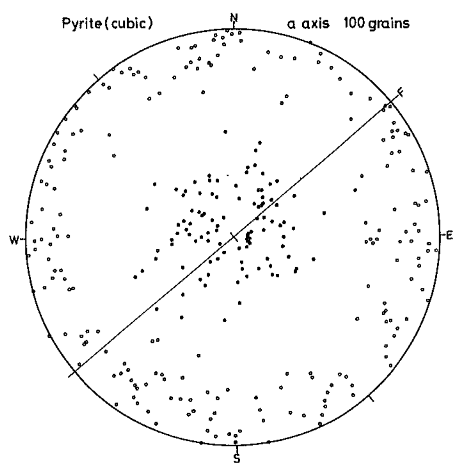

Fig. 32-(3) Pyrite fabric pattern of anthophyllite-quartz-pyrite rock facies.

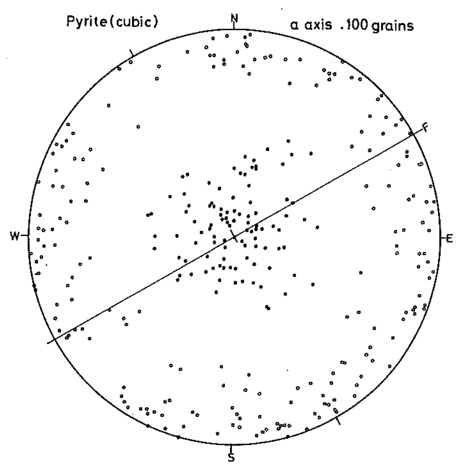

Fig. 32-(4) Pyrite fabric pattern of anthophyllite-cordierite-quartz-pyrite rock facies.

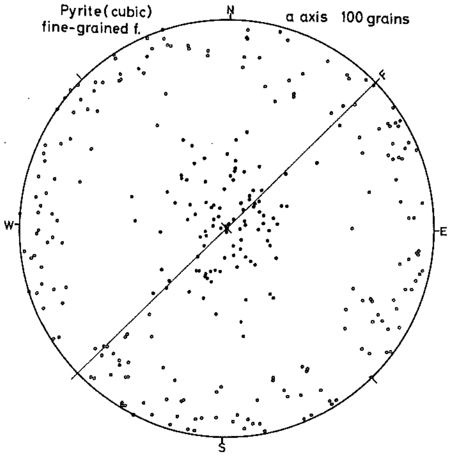

Fig. 33-(1) Pyrite fabric pattern for fine-grained facies of pyrite ore bodies at 450 ML of the Fudotaki ore bodies.

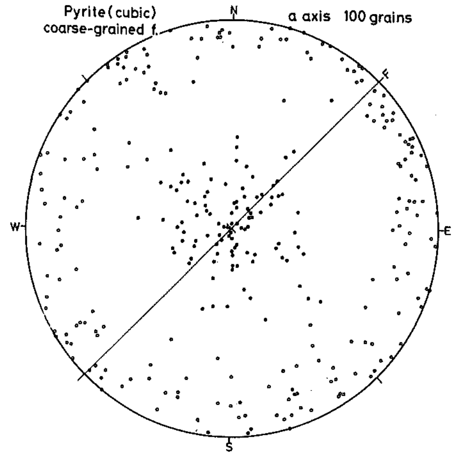

Fig. 33-(2) Pyrite fabric pattern for coarse-grained facies of pyrite ore bodies at 450 ML of the Fudotaki ore bodies.

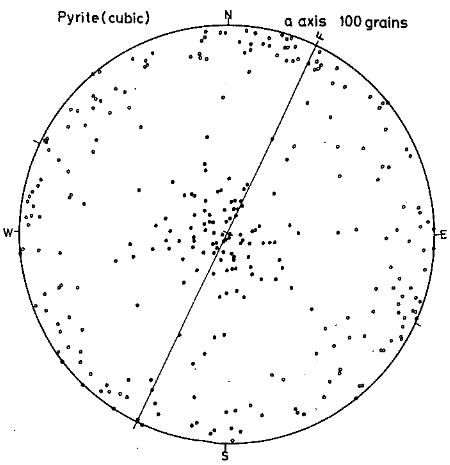

Fig. 33-(3) Pyrite fabric pattern of another pyrite ore bodies at 450 ML of the Fudotaki ore bodies.

quartz *c*-axis plots 38° from the pole of (100), viz. 52° from the pole of (0$\bar{1}$2), 19° from the pole of (201). If r(10$\bar{1}$1) is attached to (001) and the vertical plane which includes the quartz *c*-axis is either perpendicular to or parallel to the striation direction on (001), then the *c*-axis plots 38° from the pole of (100) or (0$\bar{1}$0). In recapitulation, modes indicate that the r-face of quartz is lying on the pyritohedral or cube face of pyrite, parallel or perpendicular to the pyrite striations. This gives the observed c^a angles of 12°, 26° and 38° and angles between the *c*-axis and the pole of the phyritohedral face is 0° or 19°.

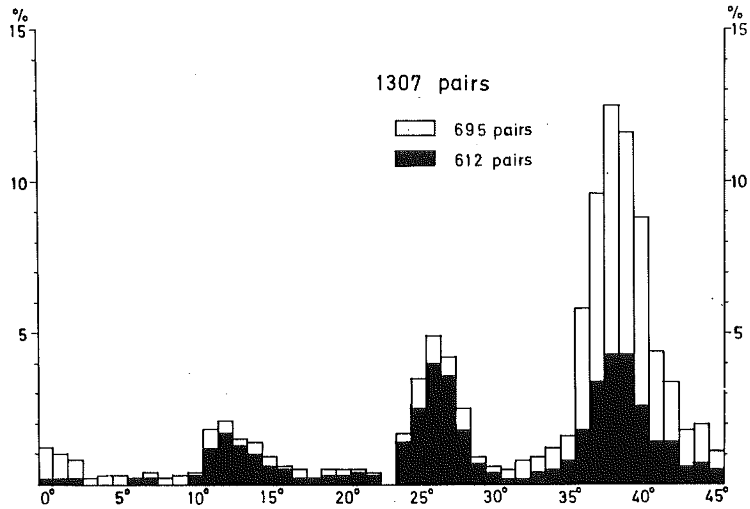

Fig. 34 A histogram of registered angles between *c*-axis of quartz and the pole of pyritohedral face (c^e: framed line), or a-axis (c^a: solid line) of pyrite in adjoining grains.

It may be possible to explain why the *c*-axes of quartz grains not only show a strong maximum in the central area of quarts fabric patterns, but also show several sub-maxima around this central position (Figs. 1, 5, 9 and 13). Measurements of pairs of adjacent grains (*c*-axis of quartz and a-axis of pyrite) are plotted in Fig. 36 on Schmidt net. From this plot it can be seen that most of the measured a-axes of pyrite are concentrated within a small circle, which implies a locus of pyritohedral face around a(001) of the central position, viz. [001]^(0$\bar{1}$2)=26°. The quartz grains show the characteristic duplicate spheroidal symmetry. Ninetyfour of the 625 measured grains (15%) fall within the small circle. The statistical distribution obtained from Fig. 36 attains a maximum concentration of 4% in the centre of the diagram (Fig. 37).

Fig. 38 is a replot of 100 of the quartz/pyrite pairs plotted in Fig. 36 but in this case the quartz grain is assumed to form oriented over growths on either the cube face(001) or the pyritohedral face($0\bar{1}2$) of pyrite and the plots have been oriented accordingly. The resultant plot should be compared with the theoretical diagram of Fig. 35.

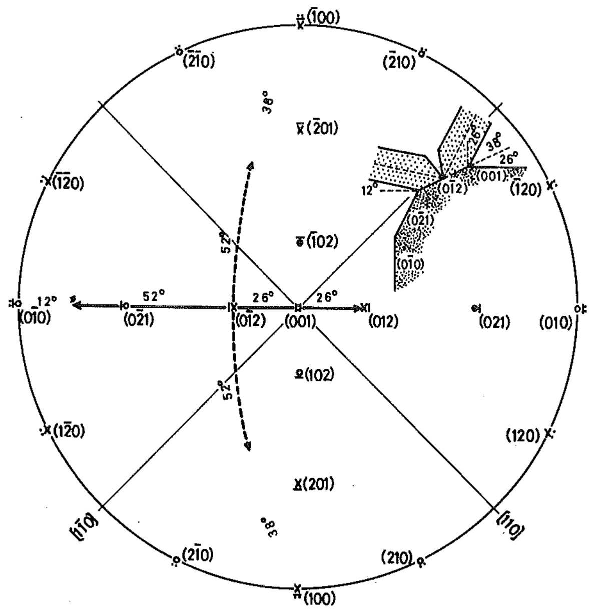

Fig. 35 A theoretical diagram representing the mutual relations between *c*-axis of quartz and pyritohedral or cube face of pyrite. A pair of pyrite crystals with pyritohedral and cube faces, twinned each other with the twin axes [110] and [$1\bar{1}0$], viz. twin after Iron Cross Law, is projected on Wulff's net. Faces marked by a cross signify one twin individual and those marked by an open circle the other. Furthermore, the striation directions demonstrated on each face are projected by the following marks, a coupling dot: the vertical direction, a short line: the horizontal direction, and a mixed mark of them signifies two possible directions in terms of Iron Cross twins.

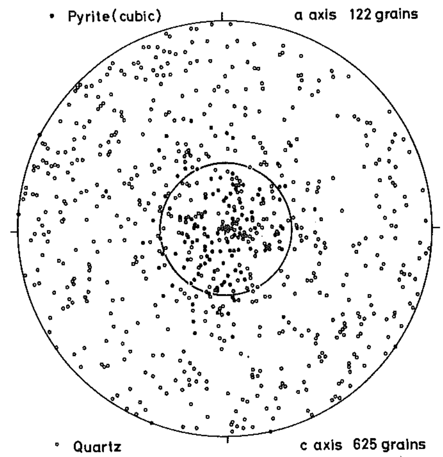

Fig. 36 An actual pattern obtained from the measured pyrite and quartz, based on Fig. 35. On Schmidt net. Small circle implies a locus of pyritohedral face around cube a(001) of the central position theoretically.

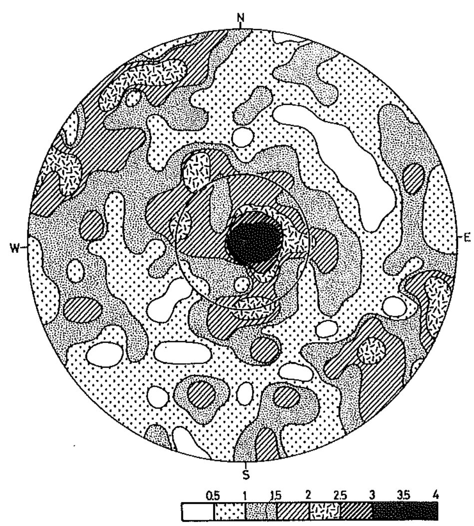

Fig. 37 An actual pattern which is statistically obtained from Fig. 36.

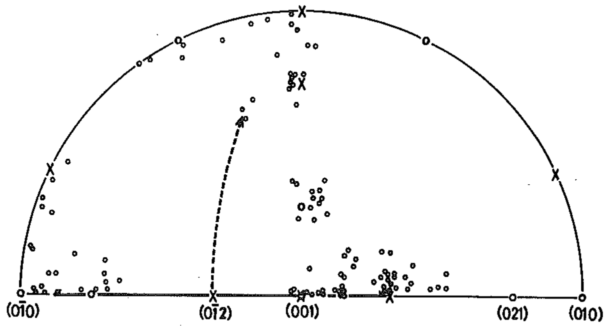

Fig. 38 An actual diagram which one hundred examples of quartz grains from Fig. 36 are exactly rearranged on cube a(001) or pyritohedral face e(012) of Fig. 35. On the northern hemisphere of Schmidt net.

These results are compatible with the actual patterns seen in Figs. 1, 5, 9 and 13 and support the idea that there may be crystallographic relations between the cube or pyritohedral face of pyrite and the *c*-axis of quartz crystals in these facies.

Since these appear to be definite crystallographic relationships between adjacent quartz grains and between adjacent quartz and pyrite grains, it seems reasonable to expect similar relationships between adjacent pyrite grains. It is possible to draw the following conclusions, according to the another work (WATANABE, in press). (i) Parallel growth arranged mutual cube faces a(001) among the pyrite grains, (ii) parallel growth arranged mutual pyritohedral faces among them, and (iii) parallel growth arranged mutual cube and pyritohedral faces among them. These relationships by the parallel growing of the identical orientation among them whether they are immediately contact each other or even quartz grains exist only a few among them, are predominantly effected. In consequence of them, some porphyroblastic domains attained up to about 2 or 3 cm in length, which are consisted of scores of the identically oriented grains of small pyrite cube or pentagonal dodecahedron, are very often formed in pyrite compact ore of the later mineralization in phase.

Summary and conclusions

(A) An alteration zone associated with the sulphide mineralization of the Hitachi copper mine is well-developed and covers a large area. The notable ore bodies are all localized in one mineralized zone, which is the most strongly altered part of the alteration zone. This zone can be subdivided into a great number of units consisting of seven different facies arranged en echélon. The following facies are identified: (1) chlorite-sericite-quartz, (2) sericite-quartz-pyrite, (3) sericite-quartz-andalusite-pyrite, (4) cordierite-quartz-pyrite, (5) anthophyllite-quartz-pyrite, (6) anthophyllite-cordierite-quartz-pyrite, and (7) anthophyllite-cordierite rock facies with skarn assemblages.

(B) The alteration took place primarily in or around sheared zones with a NE–SW trend. The fissility and lineation of these rocks are very marked, and they are readily distinguished from the wall rocks which are very different in tectonic appearance. On the whole, it may be concluded that the initial tectonic force which preceded the ore mineralization and was operating along the sheared zones, throughout the whole period of alteration, was a roughly lateral movement.

(C) Microfabric studies have been used to elucidate the rules of coordinations for the main mineral associations. The factors controlling crystallization appear to have been very similar throughout the period of hydrothermal alteration. The main results of the studies are as follows.

(1) Patterns show distinct duplicate spheroidal symmetry around one concentrated maximum. The maximum coincides with the plunge of the shoot of ore bodies. A few sub-maxima were separated by an angle of 25° to 26° from the main maximum.

(2) A.V.A. Contour Maps obtained topologically by contouring concentration degree in respective group based on the actual orientation and disposition of individual measured quartz grains show many fine domains which are characterized by aggregation of a few to tens of grains having identical preferred orientation. The domains have somewhat elongated form and are arranged roughly parallel, or in a few cases slightly oblique, to the foliation plane.

(3) The angles formed by the *c*-axes of two immediately adjoining quartz grains do not vary in a random manner but are concentrated in six modes at 9°, 33°, 51°, 60°, 77° and 84°. About three-quarters to two-thirds of all measured pairs fall within these six modes. Grain pairs showing one of these six "special" angles are said to be in "coordination relation". Grain pairs are distributed among the four angles 84°, 60°, 51° and 33° approximately in the ratio 1:1:1:1. This observed result is in good accordance with the theoretical ratio assuming most of quartz to be present as three or four component twins.

(4) Adjoining grains belonging to the mode at 84° may be interpreted as being in "Japanese twin" relationship, because twinned crystal of quartz with composition plane $\xi(11\bar{2}2)$ and an angle of 84°33′ between the *c*-axes across are usually known as "Japanese twins".

It has been shown earlier that the angles 60°, 51°, 33° and 9° will also be produced when multiple Japanese twinning occurs.

(5) The concentration degree at the mode of 77° is even higher than that of the other five modes, but this cannot be explained in terms of Japanese twinning. It may be interpreted as indicating the existence of twinning after the "Estérel law" with twin plane $(10\bar{1}1)$ and c-axes intersecting at an angle of 76°26′.

(6) The characteristic fabric pattern of duplicate spheroidal symmetry was analysed to see if it would be explained on the basis of twinning. It was confirmed that widespread twinning after the Japanese law could be expected to produce just this type of fabric pattern. Judging from Fig. 20, in which most of the Japanese twin-planes are concentrated on a circle with radius of about 40° around the centre of diagram but some are positioned perpendicular to the perimeter, one can consider a series of Japanese twin triplets shown in Fig. 30. If a series of Japanese twin triplets are produced and all have the c-axis of one twin component vertical the twin-plane pattern would be of the type observed in Fig. 20 whilst the c-axis pattern would be one of duplicate spheroidal symmetry.

(7) With regard to pyrite grains which are present in variable amounts in the alteration facies, their relations to adjoining quartz grains were studied, because it could be important to know how pyrite grains filling the interstices are affected by the fast coordinations established by the quartz grains. It was found that the angle between the c-axis of quartz and pole of the cube and pyritohedral faces is 38°, 26°, (19–21°), 12° or 0°. This certainly means that in spite of being attaching along irregular boundaries there is some crystallographic control on the relative orientation of these pairs.

(8) Since there are several definite coordination relations, not only between quartz grains but also between quartz and pyrite grains, it seems reasonable to investigate the possibility of similar relationships among adjacent pyrite grains.

(D) The theory that the unique fabric patterns observed in these facies may be due to multiple twinning and other crystallographic controls of grain orientation has been tested and found to fit the observed data. If this explanation of the fabric is correct a number of questions arise among them.

a) Why has the occurrence of Japanese and Estérel twinning been so common throughout the period of alteration?

b) Why has one grain in each twin group a given orientation when the tectonic environment during formation is one of lateral movement?

c) What is the reason for the rather special type of coordination observed between quartz and pyrite?

(E) Pyrite like quartz has a strong tendency to be oriented so that one crystallographic axis corresponds to the plunge of the ore shoot of the ore body which suggests an intimate genetical connection among ore body, alteration and tectonic environment.

Acknowledgements

Professor M. HUNAHASHI, who has for long years pursued the thesis on mineral coordination throughout alteration processes taking part in ore mineralization of several mines, granted me the problems discussed in present paper. I here wish to extend my sincere thanks to him for stimulating discussion and his valuable guidance.

Several important arguments for a lot of problems met with during investigation are given by Professor S. HASHIMOTO, Drs. M. KUMAZAWA, C.W. KIM, Y. OHTA, T. TSUCHIYA, Messrs. S.G. HOE, S. SUGIYAMA and H. SHIMAOKA.

I should especially like to thank the Nihon mining Company afforded facilities for my field survey of the Hitachi mine since 1966.

I am also much indebted to Professor S. Gavelin, Dr. R. RUSSELL and Mrs. B. JENSEN for kindly reading manuscript and their valuable suggestions.

References

FAIRBAIRN, H.W. (1949): Structural petrology of deformed rock. Cambridge.

GOLDSCHMIDT, V. (1897): Kristallographische Winkeltabellen. 432p. Berlin.

GOLDSCHMIDT, V. (1920): Atlas der Kristallformen, "Pyrit". Bd.VI. Heiderberg.

GOLDSCHMIDT, V. (1923): Atlas der Kristallformen, "Quarz". Bd. VII. Heiderberg.

HUNAHASHI, M. (1973): Quartz Fabrics in an Epithermal Ore Vein. Contr. Miner. Petr., vol.39, no.2, p.157-170.

KOTO, B. (1892): The Archean formation of the Abukuma plateau. Jour. College Sci., Imp. Univ., 5,3,p.197-291.

KOZU, S. (1952): Japanese Twin of Quartz. Amer. Jour. Sci., Bowen Volume, p.281-292.

MINATO, M., GORAI, M. and HUNAHASHI, M. (1965): The geologic development of the Japanese Island. 442p, Tokyo.

MINATO, M. (1968): Basement complex and Palaeozoic orogeny in Japan. Pacific Geology, 1,p.85-95.

SUGI, K. (1935): A preliminary study on the metamorphic rocks on southern Abukuma plateau. Jap. Jour. Geol. Geogr., 12,p.115-151.

TROMMSDORFF, V. und WENK, E. (1963): Diskussion eines Zwillingsgefüeges durch Achsenverteilungsanalyse an Quarz eines Tessinergneisses. Schweiz, Min. Petr. Mitt., Bd.43,H.2,p.687-698.

WATANABE, J. (1971): Petrofabric analysis on the Basement Complex of the Southern Abukuma Plateau, Japan. Pacific Geology, 3,p.67-93.

WATANABE, J. and BIKERMAN, M. (1971): K-Ar age of the Nishidohira gneiss complex in the Abukuma mountains, Japan. Earth Science (Chikyu Kagaku), 25,p.23-26.

WATANABE, J. (in press): Lattice fittness of neighbouring pyrite grains in pyrite porphyroblastic domains in certain ores. Jour. Fac. Sci., Hokkaido Univ., Ser.IV, Geol. Miner.

WATANABE, M. (1920, 1921): On the igneous rocks in the Hitachi Mine and their relation to the ore deposits (in Japanese). Jour. Geol. Soc. Japan, 27,p.441-450, p.477-486.

WENK, H.R. (1965): Gefügestudie an Quarzknauern und -lagen der Tessiner Kulmination. Schweiz. Min. Petr. Mitt., Bd.45,H.2, p.467-515.

WENK, H.R. und TROMMSDORFF, V. (1965): Koordinatentransformation, Mittelbare Orientierung, Nachbarwinkelstatistik. Beitr. Miner. Petr., 11,559-585.

(Manuscript received on April 1, 1974)

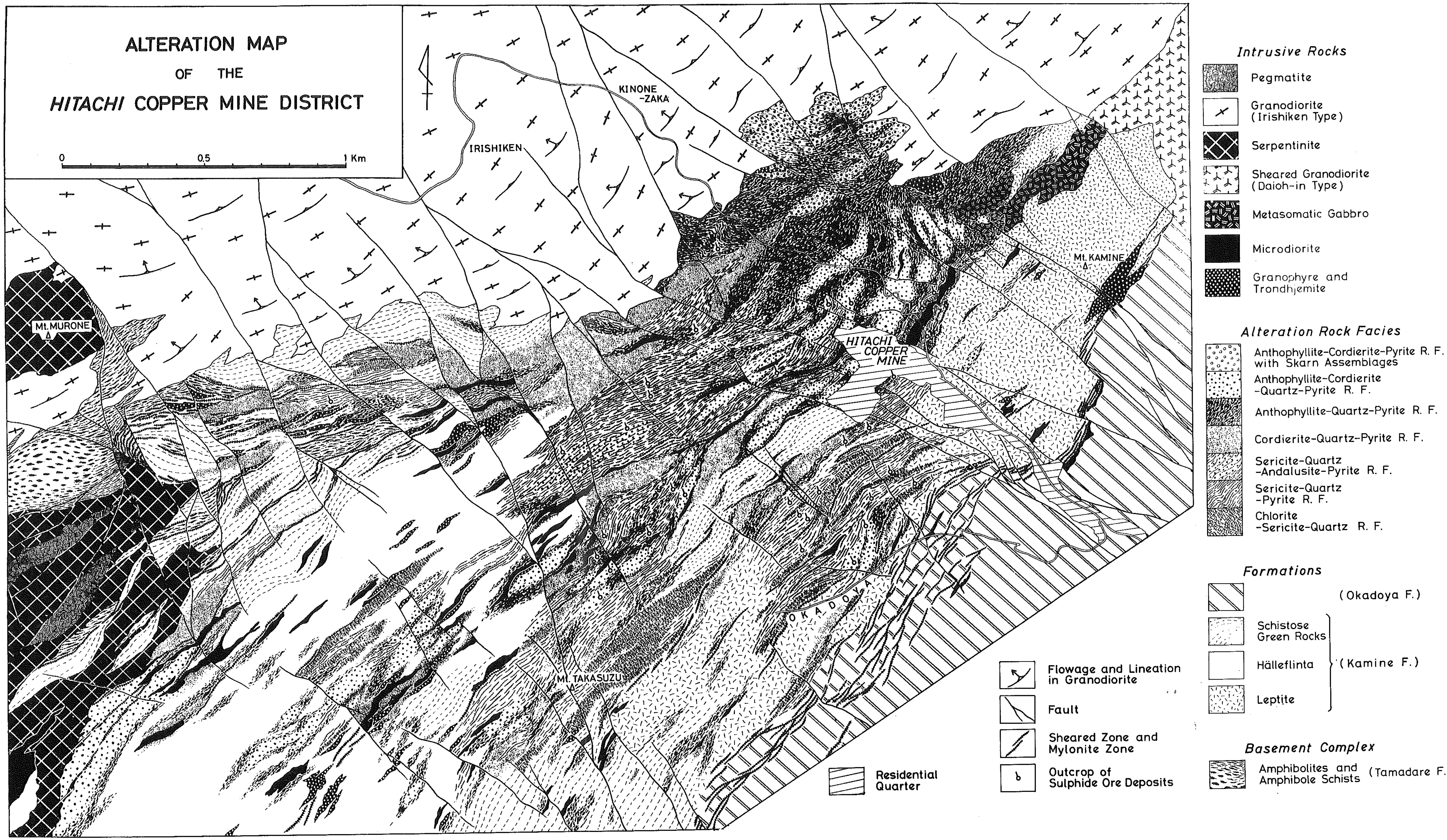

Fig. 39 Alteration map of the Hitachi copper mine, Abukuma Plateau, Japan.